Surface Decontamination using Cold Atmospheric Pressure Plasma

A Thesis
SUBMITTED TO THE FACULTY OF
UNIVERSITY OF MINNESOTA
BY

Ankit Moldgy

IN PARTIAL FULFILLMENT OF THE REQUIREMENTS
FOR THE DEGREE OF
MASTER OF SCIENCE

Adviser: Dr. Peter J. Bruggeman

June 2019

Acknowledgements

Firstly, I would like to express my sincere gratitude to my adviser, Dr. Peter J. Bruggeman, for his close guidance in the execution of my research. His patience and resourcefulness have helped me get accustomed to working in this area of plasma science with minimal prior knowledge. His supervision has taught me to work towards developing a comprehensive 'story' within the existing practical constraints to address the gaps in research.

I would also like to thank Dr. Sagar M. Goyal from the College of Veterinary Medicine for his valuable insights on the biological aspects of this study. The laboratory facilities at the Veterinary Diagnostic Lab have been instrumental in the execution of this work. I would like to extend my sincere thanks to Dr. Steven L. Girshick for his willingness to be a part of my master's thesis defense committee and the constructive interactions that followed.

I would like to thank Dr. Hamada A. Aboubakr for working with me patiently on all the pathogen treatment experiments. I have been taught the ways of dealing with sensitive equipment in a biology lab and the techniques for biological sample preparation and analysis by him. Working in two different labs has been challenging and I thank him for adapting his schedule based on my availability.

I extend my special thanks to Gaurav Nayak for playing the role of a mentor due to his prior involvement in similar areas of research. I remember running into him during my initial days in this country, and I am glad that his remark on how our interactions wouldn't stay strictly professional couldn't be more true. I would also like to thank Santosh Kondeti and Dr. Marien Simeni Simeni for their helpful interventions in the lab and the stimulating discussions that have flattened out my learning curve. I would also like to thank visiting researchers Dingkun Yuan and Wei Xiao for working with me on the measurement of reactive species in the gas and liquid phases, respectively. I have shared my office space with Mahsa Mirzaee and this has helped us work together on our coursework and plan for fun outdoor trips on several occasions.

I have deeply cherished the company of my friends Krishna Sandeep Prata, Sandeep Avvaru, Anirudh Reddy Ravula, and Vinod Kumar Avulapati during my stay in this city. Their cheerful presence has turned our place of dwelling the closest it can get to a home.

All the materials used in the experimental work were either fabricated through our own designs or purchased from external vendors. I would like to thank the staff from the CSE Shop and the ME Student Shop for fabricating the necessary parts and helping me access the necessary devices to facilitate machining, respectively. I extend my thanks to the Purchasing Department, Haewon Jun, Andrew Cahart, and Julie Gilasevich for procuring the materials used in my experimental research. I also appreciate the efforts of Richard Maharaj from the Shipping Department in ensuring the receipt of these products.

Most importantly, I would like to extend my sincere thanks to my family for being by my side through all my existence, irrespective of the circumstances. They have nurtured me with utmost love and this has had a major influence into shaping me into who I am. Finally, I would like to thank my friends back at home for being a constant support and helping me reaffirm, at the back of my mind, the simple fact that home is where the heart is.

Ankit Moldgy
28th June 2019

Dedication

This thesis is dedicated to my parents, Dr. Padmaja Madgula and Mr. Sudheer Kumar Moldgy, my brother, Mohit Sudheer, and my dear little friend, Bushy.

Abstract

Cold atmospheric pressure plasmas are being widely studied for applications in biology and medicine. Non-thermal plasma-based decontamination has been one of the important areas of investigation due to the capability of cold plasmas to generate reactive species with antimicrobial properties close to room temperatures. Foodborne viruses and bacteria have been major causes of disease outbreaks, especially through the consumption of minimally processed foods and fresh produce. Conventional non-thermal food processing technologies face limitations and affect the properties of food. This work on plasma-based decontamination was motivated by the necessity to develop an effective and efficient non-thermal food decontamination technology.

We used different plasma sources operating in air at atmospheric pressure for surface decontamination experiments. These experiments were performed with feline calicivirus (FCV), a surrogate of human norovirus, and Salmonella Heidelberg on stainless steel discs as model for food contact surfaces. The substrates were treated in dry and wet surface conditions. The plasma sources were designed such that the substrates are treated either directly such that there is direct contact between the plasma and the substrate or remotely such that the reactive species in the afterglow are transported to the substrate. It was shown that humidity on the surface of the substrate strongly enhances the decontamination effectiveness. Only direct treatment was seen to be significantly effective against dry samples. All the plasma sources achieve complete inactivation of wet samples. Synergistic effects between O_3 and NO_2 in the afterglow of the DBDs was recognized through positive

control tests. With the use of a kinetic model to study the interaction among the chemical species in the afterglow of the plasma, the virucidal effects induced by the DBDs were attributed to the generation of gas-phase N_2O_5.

The influence of surface humidity was studied through the quantification of reactive species in the water layer covering the substrate. It was found that the reactive species concentrations increased as the volume of the water decreased and this effect was consistent with the observed decontamination effects. The importance of enhancing the transport of reactive species from the gas to liquid phase for optimal decontamination efficacy of remote plasma treatment was identified.

Finally, plasma sources were compared based on the energy consumption requirements for achieving complete decontamination. To gain an understanding on the possibilities of adoption of plasma technologies by the food industry, the plasma sources were compared with UV-C radiation in terms of energy costs and practical utility. For surface decontamination, direct plasma treatment was found to be four times more energy-intensive than UV-C treatment. A significant enhancement of energy efficiency was achieved using remote plasma treatment in a lab-scale batch reactor prototype employing a surface discharge generating predominantly O_3, leading to energy per unit area requirements similar to that for UV-C. Preliminary estimates suggest that the energy efficiency might be further increased for a source enabling disinfection by reactive nitrogen species.

Table of Contents

List of Tables

List of Figures

Introduction

Plasmas are a fundamental state of matter with higher energy than the gas phase which mainly exist in space and are also extensively used in the industry for material processing. Plasmas are ionized gases, excited by thermal or electrical energy, containing a myriad of species including free electrons, ions, excited species, radicals and molecules. In spite of the presence of free electrons, a plasma is a quasi-neutral medium – in a sufficiently large volume away from the electrodes, the charge density is, in good approximation, zero. Plasmas can be categorized based on their degree of ionization, i.e., ratio of the number density of charged particles to the number of all the heavy particles. As the degree of ionization increases, Coulomb collisions between charged particles tend to dominate electron-neutral collisions. Typically, when a gaseous medium is excited by an electric field, most of the energy is transferred to the free electrons. These electrons, accelerated by the electric field, reach sufficient kinetic energies to enable the ionization of the background gas, i.e., electrons in collisions with neutral species generate an additional electron and ion. Electron-neutral collisions lead to very inefficient energy transfer compared to the energy transfer of the electric field to the electrons due to the large mass differences between the electron and neutral species. This enables a strong non-equilibrium in reduced pressure or transient atmospheric pressure plasmas. In many cases, the bulk gas temperature remains close to the ambient, while the electron temperature can be very high.

The generation of these ‘cold plasmas’ enables their application in areas of biomedicine where heat-sensitive substrates are treated with plasmas [1]. The production of reactive

oxygen and nitrogen species using cold plasmas generated in air is the main driver for their bio-medical applications [2]. The field of biomedical applications has seen a huge rise in research efforts towards surface and water decontamination, wound healing and sterilization, and also cancer therapy [3]. The interaction between plasma and living cells is complex due to the multitude of chemical species generated and the intrinsic complexity of the cell biology [4]. Many of the plasma-generated species interact with the biological substrates and can induce secondary biochemical reactions, leading to antimicrobial activity under suitable conditions. Treatment of these substrates can be performed in three modes: direct, remote, or indirect. In case of direct treatment, the biological substrate acts as one of the electrodes and the discharge generated is in direct contact with the surface of the sample. In a remote treatment setup, however, it is the discharge effluent with the chemical species that is made to interact with the substrate. Indirect treatment often refers to treatment of water or solutions that are subsequently added to biological substrates. A large variety of plasma sources have been studied for their decontamination capabilities and the associated chemistry is strongly dependent on the plasma source design and the experimental conditions. Due the added complexity induced by the large possible variety of chemical species generated in plasmas, there is currently no thorough understanding of the reactive species that are ultimately enabling plasma-induced decontamination. Further complications arise due to the dependence of plasma-substrate interaction on the presence of a water layer on the sample.

This thesis describes a broad comparative study on the antimicrobial efficacies of atmospheric pressure plasma sources. Different dielectric barrier discharges (DBDs) and gliding arc discharges operated in air have been used to decontaminate virus and bacteria samples on metal surfaces. A DBD operating in ambient air was used to demonstrate direct treatment of the substrates while the majority of the remote plasma treatments were performed using dry air on pathogen samples in flow-through reactors where a one-time interaction is allowed between the reactive species and the substrate.

The consumption of minimally processed foods and fresh produce has been on a steady rise. Contamination of these food products by viruses and bacteria has recurrently been the cause of epidemics and pose a real threat to public health [5], [6]. Conventional non-thermal food processing techniques often contribute to undesirable effects or face severe limitations or disadvantages [7]. The motivation for using plasmas for disinfection arises from the need to develop an effective and energy-efficient non-thermal surface and food decontamination technology. The objective of this work is to assess the applicability of different plasma sources for the inactivation of virus and bacteria. We intend to seek answers to the following questions:

- How do cold atmospheric plasma sources with different generation approaches compare in terms of their decontamination efficacies?
- What is the dominant chemical pathway responsible for surface decontamination using remote plasma treatment?

- How does the effectiveness of decontamination using remote plasmas depend on the humidity on the surface of the substrate?
- How do the operational costs involved in the utilization of plasmas compare with the costs of UV-C, a conventional non-thermal decontamination technology?

The outline of this dissertation is as follows. Chapter 1 provides a comparison of plasma-based disinfection by direct and remote plasma sources operating in air at atmospheric pressure. To gain a better understanding of the plasma parameters appropriate for effective decontamination, it is necessary to gain a more detailed knowledge of the plasma-generated species that enable plasma-based decontamination. Chemical kinetics modeling of the plasma effluent and positive control tests were used to identify the dominant chemical pathway towards disinfection.

It has been reported that the presence of water on the surface of the biological substrate significantly enhances the efficacy of plasma-based decontamination. We observe a dependence of the antimicrobial activity on the amount of liquid covering the substrate. In chapter 2, the concentrations of reactive species in the liquid layer were quantified using colorimetric techniques to correlate the observed antimicrobial effects with the aqueous-phase species concentrations. The significance of optimizing the gas-to-liquid phase transport of the reactive species is recognized.

Studies reported in literature put little emphasis on the costs involved in the utilization of plasmas for effective decontamination. To facilitate the integration of this technology into the food industry, an engineering perspective is required to provide estimates of its

operational costs and suggest means of optimization. In this regard, chapter 3 assesses the benefits and drawbacks of using different DBDs and the conventional UV-C technology for decontamination in terms of their energy consumption and practical utility. A batch reactor prototype was developed and tested to enhance the energy efficiency of plasma-based disinfection systems.

Finally, the main findings and conclusions of the work are summarized.

Chapter 1. Inactivation of virus and bacteria using cold atmospheric pressure air plasmas

1.1. Introduction

Cold atmospheric pressure plasmas are increasingly being investigated for the treatment of heat-sensitive surfaces with applications in biology and medicine [1–4] as they generate high reactivity near room temperatures. When the plasma is generated in air, a myriad of reactive oxygen and nitrogen species (RONS) are produced including O_3, $O_2(a^1\Delta_g)$, NO, NO_2, HNO_3, HNO_2, $ONOO^-$, H_2O_2, and OH. Many of these plasma-generated chemical species interact with organic matter and can induce secondary biochemical reactions leading to antimicrobial action [1].

Foodborne viruses and bacteria have been major causes of epidemics in the society especially through the consumption of fresh agricultural produce. Enteric viruses, such as Human Norovirus (HuNoV), are a real threat to public health due to outbreaks of diseases like acute non-bacterial gastroenteritis [5]. About 48% of all foodborne disease outbreaks attributed to a single known cause and reported to the Centers for Disease Control and Prevention from 2009 to 2012 were caused by HuNoV [6]. The bacterial pathogen Salmonella, transmitted through ready-to-eat plant produce, vegetables, poultry, and water, accounts for about half of the outbreaks caused by bacterial pathogens [7], [8].

Existing non-thermal food processing technologies have distinct limitations, such as affecting the rheological properties of food, requirement for smooth surfaces, or production

of toxic by-products. Hence, there is an urgent need to develop a non-thermal processing technology to decontaminate food and plasma has been suggested as a viable technology [9].

The identification of the underlying mechanisms of the plasma-induced disinfection process is often complex due to the possible cumulative action of the ‘cocktail’ of many different reactive species [1]. The composition of this cocktail can be strongly dependent on the plasma device and operational parameters. The chemical mechanism is further dependent on the nature of interaction of the chemical species with the substrate being treated and the different pathogens [10], [11].

Depending upon how the plasma-generated species are delivered to the substrate, plasma treatment setups can be classified into direct or remote treatment. For direct treatment, plasma is generated between the powered electrode and a sample that acts as the opposite electrodes. There is thus direct contact between the sample and plasma and large fluxes of short and long-lived species are delivered to the biological substrate. Remote plasma treatment involves the generation of the plasma at a remote location with respect to the sample and reactive species are transported by a gas flow through the plasma to the sample. For typical conditions, the gas residence time is larger than the lifetime of short-lived species, and hence it is the long-lived species present in the plasma effluent that interact with the organic substrate.

Direct discharges at atmospheric pressure have been effectively employed for disinfection of bacteria [12]–[15] with efforts to qualitatively study the role of reactive species. Gupta

et al. [12] achieve complete decontamination of *Pseudomonas Aeruginosa* in biofilms using a dielectric barrier discharge (DBD) and a plasma jet within a treatment time of 15 minutes. Fridman *et al.* [13] utilize direct discharges to study the mechanism of inactivation of *E. Coli* samples. Lu *et al*. [14] studied the dependence of the bactericidal role of charged species and radicals on the feed gas. A number of studies have established the dominant role of charged species and the negligible role of UV and heat generated towards microbicidal activity for direct plasma treatments [10], [13], [15].

A few studies employ point plasma sources like plasma jets for the purpose of disinfection [2], [16]–[18], but there are obvious practical advantages favoring large-area plasma sources that can also be scaled up eventually. Nayak *et al*. employed a two-dimensional array of microdischarges (2D DBD) [19], [20] that was extremely effective against feline calicivirus on metal surfaces covered with a layer of water and in the bulk liquid [21]. The remote treatment approach performing gas-phase treatment of the virus coated on surfaces was largely independent of the exposure distance when the treatment was performed in a flow-through reactor, suggesting that the virucidal effect was due to long-lived species. Van Gils *et al*. attributed liquid-phase bacterial inactivation caused by a remote atmospheric pressure RF jet to generation of peroxynitrites, nitrous acid, and hydrogen peroxide [2]. Lukes *et al*. showed that while a low pH of the solution is not a factor leading to inactivation of bacteria by itself, a low pH is essential for inactivation when reactive nitrogen species are drivers of the inactivation mechanism [3]. Gliding arc discharges, which are a rich sources of reactive nitrogen species (RNS), have been utilized against

bacteria and virus on surfaces and in liquid media with considerable success [11], [22]–[24]. Dasan *et al*. [11] used a gliding arc reactor to decontaminate different food contact surfaces against *E. Coli* and *Staphylococcus epidermidis*. El-Aragi [22] report significant inactivation of HCV in human blood samples by a DC gliding arc. In addition, surface discharges were used in batch reactor systems to contain the reactive species generated for the treatment of bacteria [25]–[28]. The authors reported the occurrence of two different modes of operation, an O_3-dominated low power mode and a NO_x-dominated high power mode. The inactivation of bacteria in a solution could, in this case, clearly be correlated with the aqueous phase O_3 concentration, which was also shown to be mass transfer limited. While several studies report disinfection applications of a large variety of plasma sources, there is currently no comprehensive understanding of the reactive species that are ultimately responsible for the observed antimicrobial effects.

In this study, we report on plasma-based inactivation of feline calicivirus (FCV), which is a surrogate for Human Norovirus [29], and *Salmonella Heidelberg*, motivated by this societal need. In addition, we compare the effectiveness of direct and remote plasma treatment setups in inactivating FCV, and *Salmonella Heidelberg*. All the plasma sources were generated by the same AC HV power supply with dry air as the feed gas for the remote plasma treatment conditions. We seek to identify the role of plasma-generated species for the remote treatments to gain a better understanding of the appropriate plasma parameters required for effective and energy-efficient disinfection of food and food-contact surfaces.

This chapter provides a detailed comparison of the plasma-based disinfection of four different atmospheric pressure plasma discharges operated in air. Section 1.2 describes the experimental setups used for plasma treatment of pathogens, the methods involved in pathogen sample preparation and its analysis, and the techniques for the measurement of reactive species. Section 1.3 describes the positive control tests performed on the virus samples to understand the synergistic effects among the species in the plasma effluent. In section 1.4, we discuss the time-resolved kinetic model implemented to investigate the composition of the plasma effluent the pathogen samples were exposed to. The experimental results are reported in section 1.4, and the key conclusions are presented in section 1.5.

1.2. Experimental Setup and Methods

1.2.1. Plasma treatment setups

The plasma sources and treatment configurations used in this work are illustrated in figure 1.1. A DBD referred to as the direct DBD (figure 1.1(a)), was used to provide direct treatment of the samples. The plasma source consisted of a copper rod of 25.4 mm diameter that acts as the high voltage electrode embedded in a polytetrafluoroethylene (PTFE) tube. One end of this electrode was covered with a 380 μm thick sheet of alumina. At a distance of 2 mm from the dielectric sheet, a stainless steel disc with a diameter of 11.4 mm, acts as the counter electrode. The steel disc was placed on top of a grounded aluminum plate covered by a sheet of alumina of thickness 380 μm. The surface of the metal disc facing

the discharge was spiked with the pathogen sample (see further). The plasma source was operated in ambient atmospheric pressure air and this led to the generation of a filamentary discharge over the sample. For remote treatments of the substrates, dielectric barrier discharges and gliding arc discharges were used in a flow-through reactor configuration. The array of micro-hollow dielectric barrier discharges (2D DBD) (figure 1.1(b)) consisted of an array of 105 holes with a diameter of 600 μm. A micro-discharge was generated in each hole through which dry air was flown along the inter-electrode gap with a gas residence time of 164 μs. The reader is referred to [19] for a more detailed description of the plasma source. The volumetric DBD (figure 1.1(c)) consists of five parallel rectangular gaps with a thickness of 1.75 mm and a length of 44 mm through which dry air is fed. The high voltage and grounded electrodes were embedded in the dielectric material across the rectangular gaps in an alternating manner. While we apply the same power to the 2D DBD and the volumetric DBD, the volume of the discharge region is 1280 times smaller in the 2D DBD. This leads to a much higher power density and a different plasma chemistry is expected. Two different gliding arc reactors were used to provide treatment of the samples in a wide power consumption range of 10-70 W. The reactors (figure 1.1(d)) enabled the generation of a 'gliding arc' between two diverging electrodes placed in a cuboidal space. At the position of minimum gap distance between the electrodes, the electric field is maximum, and the discharge is ignited and blown along the diverging electrodes by the feed gas (dry air). The gliding arc, due to the higher temperatures, was chosen to perform treatments mainly through the action of RNS. Both the remote DBDs and the gliding arc discharge were driven by AC sinusoidal voltage waveforms with a frequency of 20 kHz.

All the plasma sources were driven by a high-voltage AC power supply (PVM500). The direct DBD was driven by an AC sinusoidal voltage waveform at a frequency of 25 kHz and duty cycle modulation of 20% at ~100Hz. Both the remote DBDs and the gliding arc discharge were operated at a frequency of 20 kHz, while the volumetric DBD was modulated at ~100 Hz with a duty cycle of 30%.

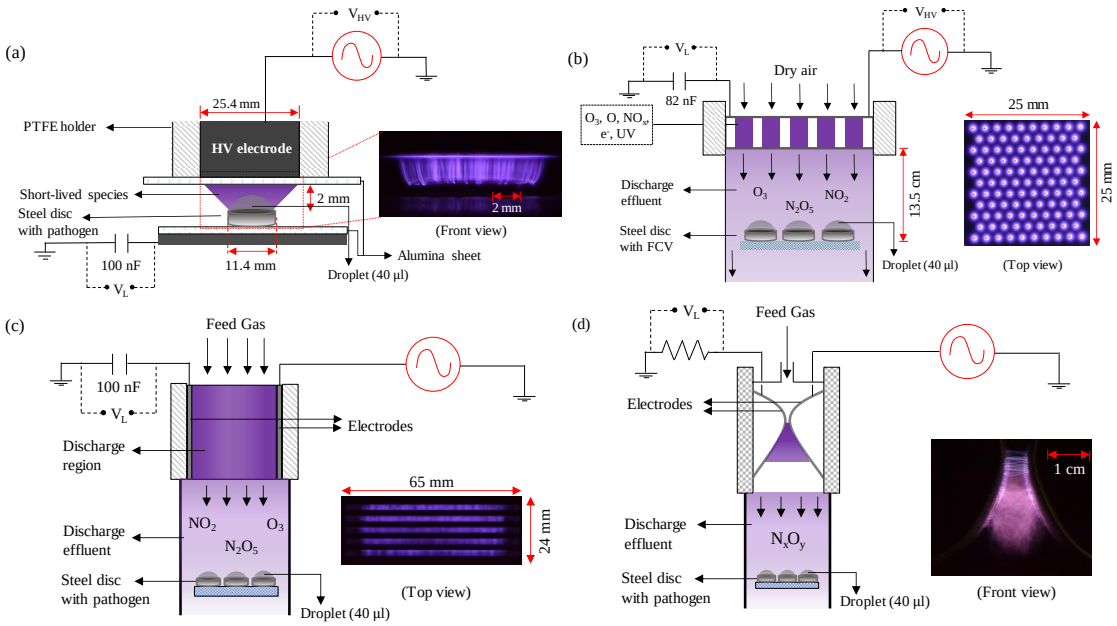

Figure 1.1. Schematic of the plasma sources in operation for the treatment of wet samples as illustrated by the water droplet of 40 µl on the surface of the metal disc. (a) Direct DBD at 12 W, (b) 2D DBD at 14.5 W, (c) Volumetric DBD at 14.5 W, and (d) Gliding arc from 10–70 W. During indirect plasma treatment, the sample holder was placed within an enclosure tube on the downstream at a distance of 13.5 cm.

Plasma sources providing a remote treatment had a polycarbonate tube of diameter 52 mm attached to the bottom of the electrode assembly. The pathogen samples were treated with the discharge effluent downstream of the plasma sources, at an exposure distance of 13.5 cm. The enclosure was used to minimize radial losses of the reactive species to the ambient

before they reached the sample location. Three samples were placed on a PTFE block and were treated by the long-lived reactive oxygen and nitrogen species in the plasma effluent.

1.2.2. Power measurement

Electrical characteristics of the discharges were studied using a Tektronix DPO2024B oscilloscope. The voltage applied to the plasma sources was monitored using a Tektronix P6015A HV probe. In case of the DBDs, the lower voltage connections were grounded through a capacitor with a capacitance at least 100 times larger than the capacitance of the plasma reactor. The power deposited into the plasma during each voltage cycle was determined using the charge-voltage plot, as described in [19]. For the gliding arc discharge, the lower voltage connection was grounded through a shunt resistor to enable the measurement of the discharge current. The average product of the voltage and the current in the plasma was used to compute the discharge power. The voltage across the capacitor or resistor were recorded using a Tektronix TPP0200 voltage probe.

1.2.3. Pathogen sample preparation and treatment

Aliquots of the pathogens were spread aseptically on the surface of sterile stainless steel discs. Surfaces of the steel discs were treated in dry and wet conditions. For treatment of wet samples, 40 µl of distilled water was pipetted onto the surface to cover the virus or bacteria stain. Plasma treatment of the pathogen samples were performed in triplicates, and the averaged results were presented along with the associated uncertainty (standard deviation).

1.2.3.a Virus assay preparation and titration

Feline calicivirus (strain 255) was grown and titrated in Crandall-Reese Feline Kidney (CRFK) cells. The CRFK cells containing the virus were incubated at 37 ^{o}C, under 5% CO_2 for 2-3 days after infection. During this period, cytopathic effects (CPE) appear and can be observed under an inverted microscope. The infected cells were frozen and thawed thrice, and then centrifuged to remove the supernatant. The remaining virus pellet was diluted in 1 ml of sterile distilled water, aliquoted and stored at –80 ^{o}C for further use. The method used for growing CRFK cells and extraction of the virus can be found in [16].

On the day of the experiments, a stock FCV suspension with around 9 $\log_{10}$ $TCID_{50}$/0.1 ml was diluted in sterile distilled water to ~5 $\log_{10}$ $TCID_{50}$/0.1 ml of eluent. Stainless steel discs with a diameter 11.4 mm were sterilized and placed in the wells of a 24-well microtiter plate. One surface of each disc was spiked with 15 µl of FCV and stored for over 30 minutes under air flow in a biosafety cabinet to allow drying.

After the plasma treatment, the metal discs were recovered in sterile dilution tubes with 1 ml of Phosphate Buffered Solution (PBS). The tubes were vortexed for at least 30 seconds to disperse all virus from the disc into the solution. For virus titration, serial 10-fold dilutions of samples were prepared by adding 20 µl of vortexed sample to 180 µl of minimum essential medium (MEM) containing 4% fetal bovine serum (FBS) in 3 wells per sample. The virus dilutions were inoculated onto the monolayers of CRFK cells in 96-well microtiter plates using 3 wells per sample. The microtiter plate was incubated at 37 ^{o}C, 5% CO_2, and 85% relative humidity and examined for the development of cytopathic effects

for about five days. The highest dilution of the virus that produced cytopathic effects in 50% of the inoculated cells was considered as the end point. The Kärber method [30] was used for the calculation of virus titer which was expressed as 50% tissue culture infective dose per 100 µl of the eluent (log_{10} $TCID_{50}$/100 µl of eluent).

1.2.3.b Bacterial sample preparation and analysis

A multi-drug resistant *Salmonella Heidelberg* strain NS-029 was isolated from a chicken breeder farm and used for the experiments [31]. 100 µl of the stock culture, initially stored at -80 °C, was thawed and inoculated into 35 ml of tryptic soy broth (TSB) and incubated at 37 °C overnight. The working culture of *Salmonella Heidelberg* was prepared by adjusting the count of bacterial cells to 3.5×10^8 CFU/ml using sterile distilled water.

Stainless steel discs with a diameter 11.4 mm were sterilized and placed in the wells of a 24-well microtiter plate. One surface of each disc was spiked with 15 µl of the working culture of Salmonella Heidelberg and stored for over 30 minutes under air flow in a biosafety cabinet to allow drying.

After the plasma treatment, the metal discs were recovered in sterile dilution tubes with 0.5 ml of elution buffer (3% beef extract in 0.05M glycerine, pH 7.2). The tubes were vortexed for at least a minute to disperse the bacterial cells from the disc into the solution. Serial 10-fold dilutions of the samples were prepared in PBS and inoculated into plates of tryptic soy agar using the pour plate technique. The plates were incubated at 37° C for 24-48 hours after the solidification of agar. The number of residual bacterial cells was determined by taking the average number of colonies formed on two countable plates multiplied by the

dilution factor and expressed as $\log_{10}$ colony forming units (CFU) per sample. The reduction in bacterial cells due to plasma treatment was measured by the difference in the $\log_{10}$ CFU between the treated and the control (untreated) samples.

1.2.4. Gas-phase O_3 and NO_x densities

Long-lived species generated by the remote plasma sources are responsible for the antimicrobial effects caused. To identify the species leading to inactivation, reactive oxygen and nitrogen species (RONS), in particular O_3 and NO_x, generated by the plasmas were measured above the location of the biological sample holder.

Beer-Lambert's law is used to determine the absolute ozone density:

$$-ln\left(\frac{I}{I_o}\right) = \sigma N l$$

where N is the absolute ozone density, σ is the ozone cross section at 253.65 nm (1.147×10^{-21} m^2) [32], l is the absorption path length, I_o is the intensity of light detected when there is no plasma, and I is the intensity of light detected during the plasma condition under investigation.

The ozone density in the discharge effluent was measured using ultraviolet (UV) absorption spectroscopy as described in [20]. Two quartz discs were accommodated on diametrically opposite ends of the flow tube enclosure to enable the UV absorption measurement. The mercury emission line at 253.65 nm from a low-pressure mercury/argon lamp was used for absorption. The UV light, after being absorbed by the effluent, was

imaged by a quartz lens into an optical fiber connected to a broadband spectrometer (Avantes AvaSpec-2048).

NO and NO_2 were measured using a commercially-available gas analyzer (ENERAC 500, ENERAC) to estimate the concentrations at the sample location (between 10 and 15 cm from the discharge).

1.2.5. Substrate temperature measurements

The surface temperature of the samples were monitored during plasma treatment using liquid crystal temperature strips (RLC-50-30/90-10, BUA2-120/49; Omega Engineering Inc.) to measure the surface temperature of the treated sample.

1.2.6. UV-C fluence

The UV-C irradiance from the plasma was measured with a detection limit of 1 mW/cm^2 using a UV light meter (UVC Light Meter 850010, Sper Scientific Environmental Measurement Instruments, Scottsdale, AZ, USA) at a distance of 1 cm from the discharge, providing an upper limit to the UV-C irradiance the samples were exposed to.

1.3. Positive control tests

FCV samples were exposed to different controlled experimental conditions to evaluate the individual role of reactive species towards inactivation. The experimental setup shown in figure 1.2 was used to perform the positive control experiments on FCV samples. A 2D DBD electrode mounted upstream was used to generate an Ar-O_2 plasma for the production of O_3. A provision was made for adding NO_2 to this gas flow before it enters the flow

through reactor. A gas flow from a gas bottle of 500 ppm NO_2/N_2 was mixed with an Ar flow to result in a gas flow with varying concentrations of NO_2. The mixing chamber allows the interaction between O_3 and NO_2 and homogenizes the flow before it encounters the sample and was used to study the effect of species produced in reactions between NO_2 and O_3. The net gas flow rate was maintained at 5 standard liters per minute (SLM) to eliminate flow-induced differences. When both NO_2 and O_3 were added, gas flow rate carrying NO_2 and O_3 were each 2.5 SLM. The samples were placed at a distance of 36 cm from the beginning of the mixing chamber, corresponding to a gas residence time of ~6.8 seconds. Effects of individual treatment with O_3 and NO_2 were contrasted with those observed with treatment involving the same concentrations of a mixture of O_3 and NO_2. [O_3] was monitored upstream of the mixing chamber and at the location of the samples to support the kinetic model.

1.4. Modeling gas composition

Table 1.1. Chemical reactions and corresponding reaction rates involved in the kinetics of an O_3-NO_x system at room temperature.

Reaction	**Rate constant** [33]
$N_2O_5 \rightarrow NO_2 + NO_3$	$0.115\ s^{-1}$
$NO_2 + NO_3 \rightarrow N_2O_5$	$2.6 \times 10^{-18}\ m^3 \cdot s^{-1}$
$NO_2 + NO_3 \rightarrow NO + O_2 + NO_2$	$4.0 \times 10^{-22}\ m^3 \cdot s^{-1}$
$NO + NO_3 \rightarrow 2\ NO_2$	$1.9 \times 10^{-17}\ m^3 \cdot s^{-1}$
$2\ NO_3 \rightarrow 2\ NO_2 + O_2$	$2.3 \times 10^{-22}\ m^3 \cdot s^{-1}$
$NO_2 + O_3 \rightarrow NO_3 + O_2$	$3.4 \times 10^{-23}\ m^3 \cdot s^{-1}$
$NO + O_3 \rightarrow NO_2 + O_2$	$1.6 \times 10^{-20}\ m^3 \cdot s^{-1}$

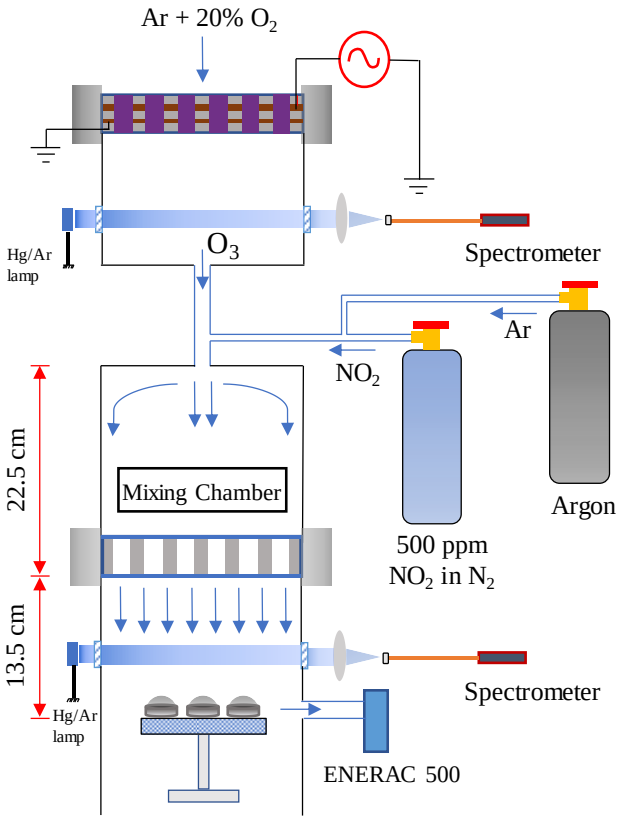

Figure 1.2. Schematic of the experimental setup used to investigate the synergistic effects arising due to the co-existence of O_3 and NO_2.

Possible synergistic effects arising from the co-existence of O_3 and NO_2 in the plasma afterglow were investigated using experiments driven by a time-resolved kinetic model. The reaction set defining the chemical mechanism was based on [33]. Table 1.1 reports the chemical reactions and their corresponding rate constants at ambient temperature and pressure. At a particular axial location, the residence time in the flow-through reactor was correlated with the axial distance from the discharge to estimate the local concentrations of species. This approach allows us to calculate accurately the evolution of species from the mixing position in the reactor (figure 1.2) up to the position of the sample. To study the

evolution of species' densities in the afterglow of the 2D DBD air plasma, the O_3 and NO_x densities at the sample location were matched with those determined from experimental diagnostics. We assumed that the plasma produces NO_2 and O_3 on the time scale of 1 ms. This timescale is short enough to be able to model the interaction among the nitrogen oxides to result in N_2O_5 but long enough not to have to consider charged and radical species [34]. It was also assumed that N_2O, although produced, does not significantly influence the NO_2, O_3 and N_2O_5 concentration due to the high stability of N_2O [34].

1.5. Results and Discussion

1.5.1. Operational parameters

Table 1.2. Operational parameters of the air plasma sources utilized for the treatment of the pathogen samples.

	Direct DBD	**2D DBD**	**Volumetric DBD**	**Gliding Arc**
Mode of operation	Direct	Remote	Remote	Remote
Reactive components	O_3, NO_x, OH, O, H_2O_2, N_2^+, O_2^+, O_2^-, UV, e^-	O_3, N_xO_y	O_3, N_xO_y	N_xO_y
Power consumption	12 W	14.5 W	14.5 W	10 – 70 W
Substrate temperature	< 70 °C (dry) < 49 °C (wet)	< 49 °C (dry and wet)	< 49 °C (dry and wet)	< 70 °C (dry) < 49 °C (wet)
UV fluence	?	< 2 $\mu W/cm^2$	< 1 $\mu W/cm^2$	< 2 $\mu W/cm^2$

To ensure that the operational parameters were suitable for the treatment of heat-sensitive food substrates, plasma conditions were chosen such that sample temperatures did not exceed 70 ^{o}C. Table 1.2 summarizes the working conditions utilized for the treatment of the samples. In the afterglow of the DBDs , O_3 and N_xO_y (NO, NO_2, NO_3, N_2O, N_2O_5) co-exist, while the afterglow of a gliding arc discharge mainly consists of NO. The ineffectiveness of the gliding arc at 14.5 W (see further) has motivated us to extend the gliding arc experiments up to powers to 70 W.

Inactivation of FCV and Salmonella due to thermal effects were known to occur due to exposure to temperatures above 63.3 ^{o}C and 57 ^{o}C for 2 minutes, respectively [29], [35]. For wet conditions, the substrate temperatures remained below 49 ^{o}C. In all the experimental conditions, although the temperature reaches up to 70 ^{o}C for some of the dry treatments by the gliding arc and the direct DBD, the samples treated with the gliding arc exhibit negligible inactivation, indicating the ineffective role of heat towards decontamination even at an exposure to 70 ^{o}C for 10 minutes. The UV-C fluence remained below 1.2 mJ/cm^2 for all the remote treatments, which is two orders of magnitude lower than the UV-C fluence needed for inactivation of the concerned pathogens [36]. The observed biocidal effects induced by remote plasmas are thus due to reactive oxygen and nitrogen species. Previous studies [10], [14], [15] reported a dominant role of charged particles and radicals, and a minimal role of UV photons and heat in case of direct discharges.

1.5.2. Comparison of decontamination by different plasma sources

Figure 1.3 shows the reduction in FCV titer induced by plasma treatment by the different plasma sources. The results show a strong dependence of the efficacy of plasma treatment on the surface humidity of the pathogen samples, particularly for remote plasma treatment. It is seen that effective disinfection of dry samples was only possible during direct contact of the discharge with the sample, while negligible virucidal effect is observed in the case of remote treatment. This result is in agreement and extends our previous study that reported the importance of surface humidity for effective operation of the 2D DBD plasma

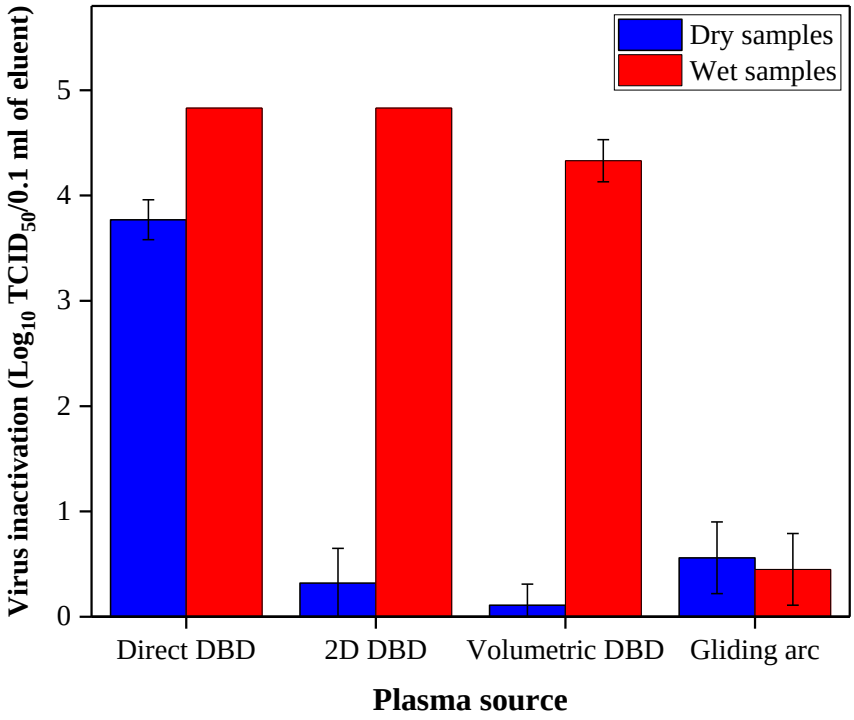

Figure 1.3. Reduction of FCV titer for different plasma sources. The effectiveness of plasma treatment on dry and wet samples are compared.
Plasma treatment time – Direct DBD: 3 minutes (dry), 5 seconds (wet); 2D DBD, Volumetric DBD, Gliding arc: 4 min (dry and wet).
Discharge power – Direct DBD: 12 W; 2D DBD, Volumetric DBD, Gliding Arc: 14.5 W

source [21]. Fridman *et al.* [13] also reported a dependence of plasma-induced inactivation on the surface humidity of *E. Coli* samples on glass slides. Similar observations were made in the literature for the disinfection of several viruses on hard and porous surfaces using gaseous ozone treatment [37], [38].

Our previous study [39] identifies oxidation of the amino acids on the virus capsid as an important pathway towards inactivation of feline calicivirus exposed to oxygen plasma, suggesting that the presence of water enhances these oxidation reactions. All the results reported hereafter in this manuscript have been obtained for wet samples only.

Figure 1.4 shows the residual virus and bacteria titer after exposure to plasma as a function of treatment time for different plasma sources. Direct contact treatment achieves complete inactivation within 5 seconds due to the enhanced virucidal and bactericidal effects of

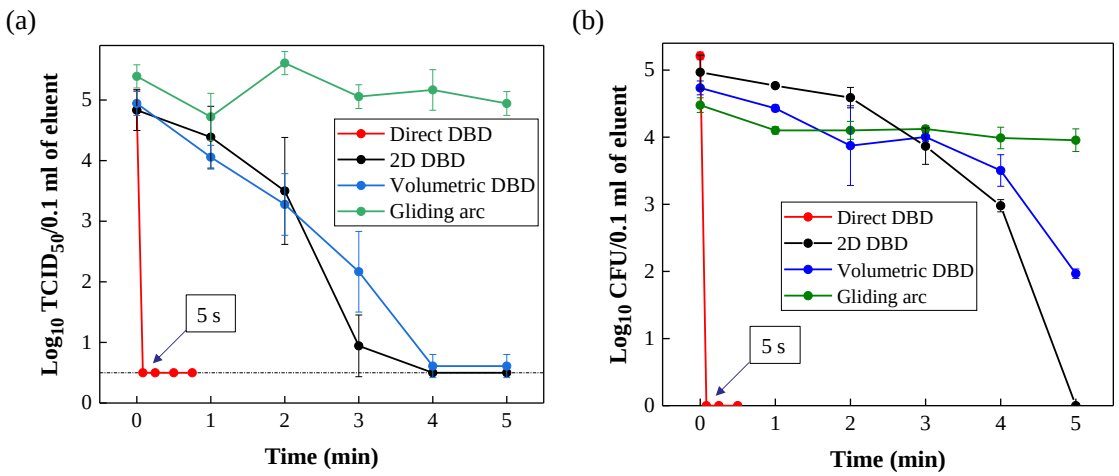

Figure 1.4. Antimicrobial effects induced by different air plasma sources on (a) FCV, and (b) Salmonella samples as a function of treatment time.
The direct DBD was operated at a discharge power of 12 W while the remote plasma sources were operated at a discharge power of 14.5 W.
The detection limit of the method for the analysis of virus titer is indicated by a dashed line in figure 1.4(a).

short-lived species. Treatments using both the remote DBDs achieve complete inactivation of FCV within 4 minutes. Longer treatment times (5 minutes for 2D DBD and even longer for the volumetric DBD) are required in case of treatment of Salmonella, suggesting that FCV is more susceptible to the plasma-generated species than Salmonella. Also, at identical power and air flow rates for the remote plasma sources, the gliding arc is remarkably ineffective against both FCV and Salmonella.

As gliding arc discharges have been successfully used for inactivation of virus and bacteria by other groups [11], [22]–[24], the decontamination efficacy of gliding arc discharge in this study was tested for increased powers up to 70 W. The inactivation observed, as a function of treatment time, is shown in figure 1.5. At a discharge power of 70 W, complete inactivation of FCV was achieved for a treatment time of 10 minutes, while Salmonella was reduced by 3.6 $\log_{10}$.

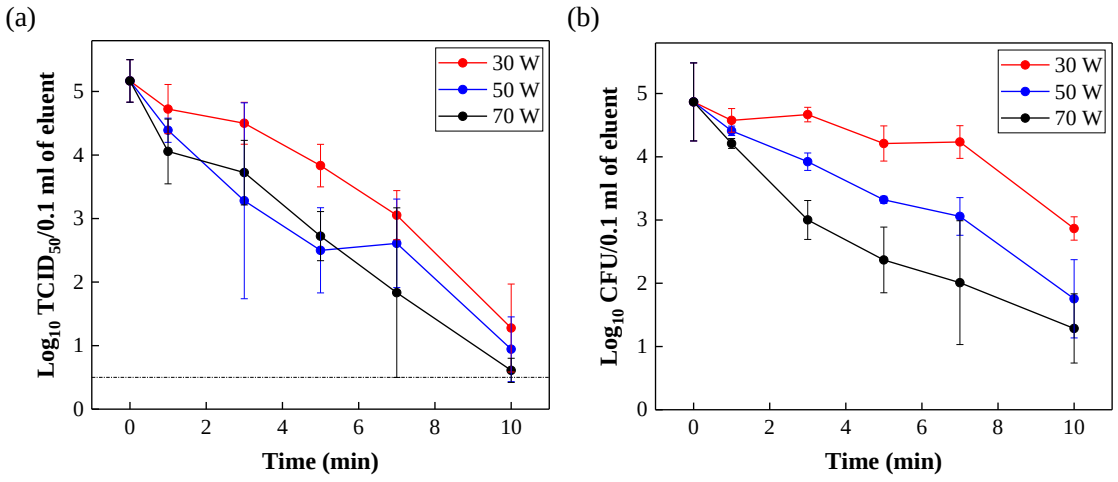

Figure 1.5. Antimicrobial effects induced by a gliding arc discharge operating on dry air as a function of treatment time on (a) FCV, and (b) Salmonella samples.
The plasma source was operated at discharge powers of 30 W, 50 W, and 70 W. The detection limit of the method for the analysis of virus titer is indicated by a dashed line in figure 1.5(a).

Figure 1.6 provides a comprehensive summary of the FCV inactivation caused by exposure to the four different plasma sources for a duration of 4 minutes. For each case, the corresponding concentrations of O_3, NO and NO_2 are also shown. Both the 2D DBD and the volumetric DBD achieve complete inactivation of the virus and produce similar concentrations of O_3 and NO_2 in their effluents. To assess the effect of O_3, we generated an Ar/O_2 plasma in the 2D DBD at conditions such that the concentration of O_3 produced was identical to the concentration of O_3 in the 2D DBD air plasma. A significant drop in the inactivation of virus was observed in the absence of reactive nitrogen species, consistent with [21]. This implies that RNS significantly contribute towards disinfection.

The gliding arc discharge exhibits very negligible virucidal effects at 14.5 W although a considerable concentration of NO is generated. The gliding arc reactor generating ~270 ppm of NO and ~35 ppm of NO_2 at a discharge power of 50 W achieved a reduction in virus titer by ~2.6 $\log_{10}$ inactivation. The difference compared to the DBDs could be explained by the Henry's law constant of NO which is about an order of magnitude lower than that of O_3 and NO_2 [40]. Even with significantly larger gas-phase concentrations of NO, RNS production in the liquid phase might be more transport-limited in case of the gliding arc. Exposure of the virus samples to a concentration of 500 ppm of NO and NO_2 for the same duration as the plasma treatment led to negligible virucidal effects in spite of the concentrations of NO and NO_2 being 2-3 times higher than that in the plasma effluent. The relatively small virucidal efficacy of O_3, NO_2, and NO suggest that other species or

synergistic effects among species in the plasma effluent contribute significantly to the observed virucidal action of the 2D and volumetric DBDs.

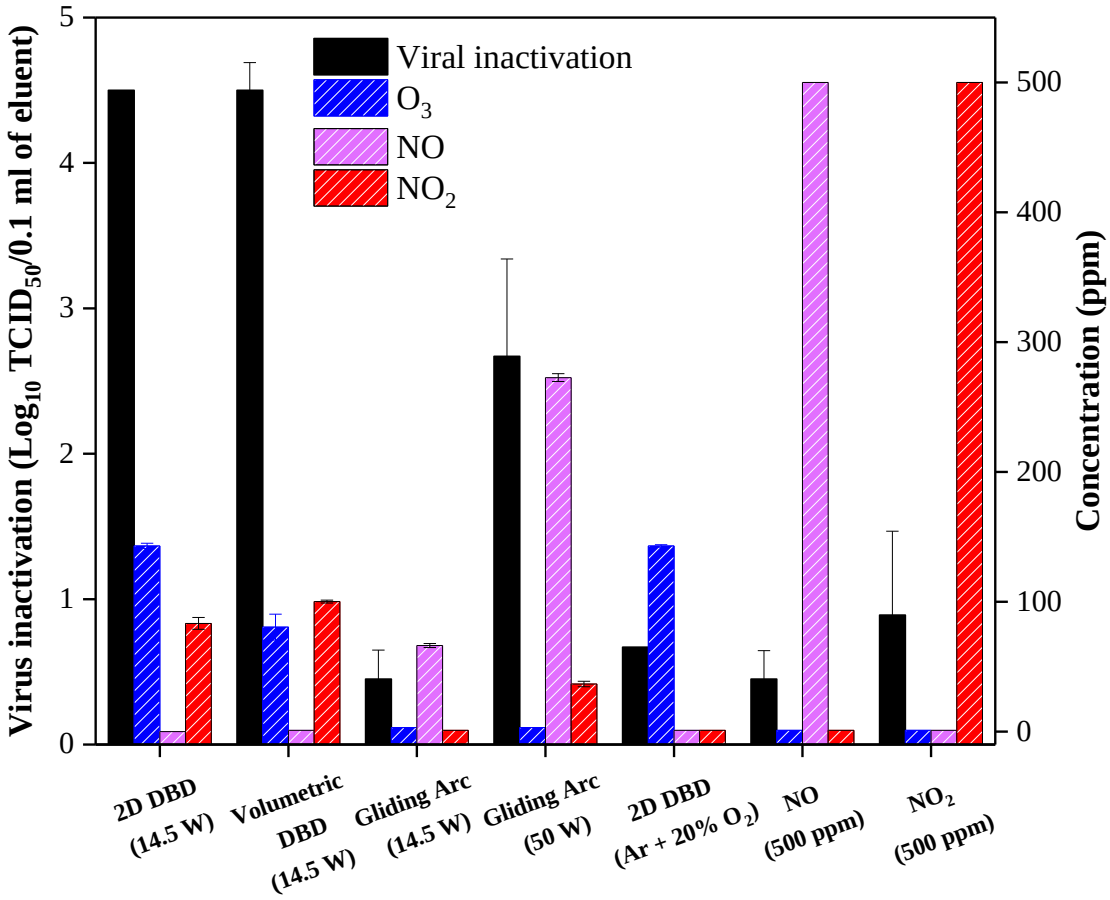

Figure 1.6. The magnitude of virus inactivation caused when FCV coated steel discs were exposed to different plasmas or gases for a fixed treatment time of 4 minutes. The concentrations of O_3, NO, and NO_2 in the effluent measured at the sample location for each of these conditions is also provided.

1.5.3. Assessing the role of N_2O_5 in virucidal activity

Figure 1.7 shows the virucidal effects induced by treatments using O_3, NO_2, and mixtures of O_3 and NO_2. The treatment conditions of figure 1.7 are summarized in table 1.3. The virus samples were exposed to a gas flow containing the species at a given concentration

for a period of five minutes. Exposure to O_3 and NO_2 led to negligible virus inactivation, while the mixture of O_3 and NO_2 with the highest concentration of NO_2 used (6.1×10^{21} m^{-3}) led to complete inactivation of the virus. This suggests a significant enhancement of the virucidal effects due to species produced by reactions of O_3 and NO_2.

Table 1.3. Gas-phase concentrations of reactive species at the beginning of the reactor and at the location of the samples for conditions utilized for the treatment of FCV samples. The results of the treatment are shown in figure 1.7. [NO_2] and [N_2O_5] at the location of the samples have been estimated from the model.

	Initial concentrations (m^{-3})		**Concentrations at the samples (m^{-3})**		
Treatment condition	**[O_3]**	**[NO_2]**	**[O_3]**	**[NO_2]**	**[N_2O_5]$_{est}$**
Air Plasma	7.3×10^{21}	9.8×10^{21}	3.5×10^{21}	2.0×10^{21}	1.4×10^{21}
O_3	10^{22}	-	10^{22}	-	-
NO_2 – I	-	6.1×10^{21}	-	6.1×10^{21}	-
NO_2 – II	-	1.2×10^{22}	-	1.2×10^{22}	-
O_3 + NO_2 – I	10^{22}	7.5×10^{20}	9.6×10^{21}	4.7×10^{17}	3.7×10^{20}
O_3 + NO_2 – II	10^{22}	1.5×10^{21}	9.3×10^{21}	1.2×10^{18}	7.4×10^{20}
O_3 + NO_2 – III	10^{22}	6.1×10^{21}	7.0×10^{21}	2.1×10^{19}	2.98×10^{21}

To determine the chemical composition at the position of the virus sample for the condition of mixing of O_3 and NO_2 in figure 1.7, we use the chemical mechanism in table 1.1 to model the change in composition of the effluent as a function of time (see section 1.4). Figure 1.8(a) shows the temporal evolution of the chemical species after mixing of O_3 and NO_2 for the initial concentrations of [O_3] = 10^{22} m^{-3} and [NO_2] = 6.1×10^{21} m^{-3}. The

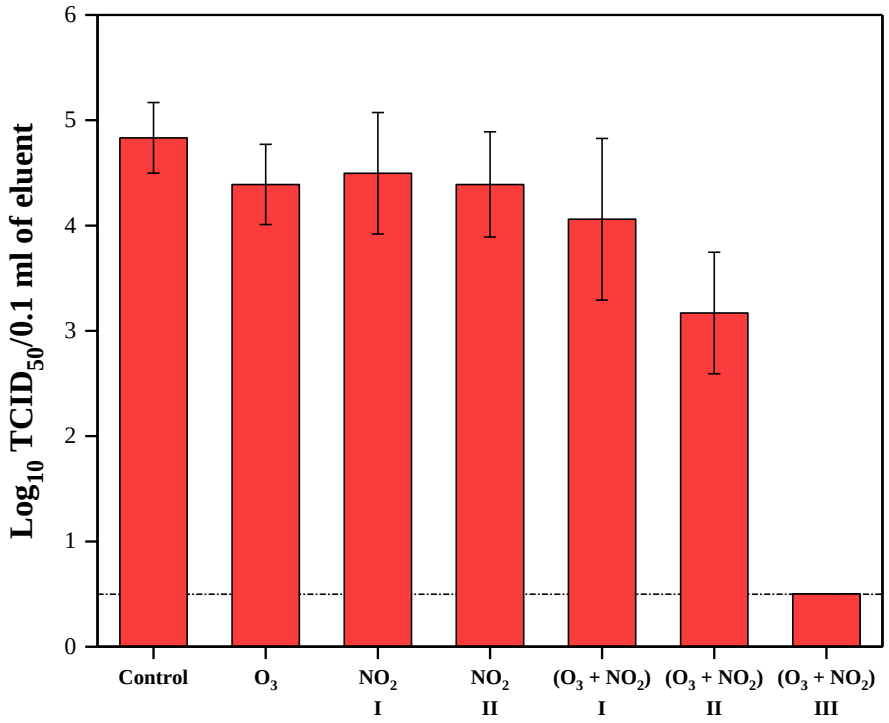

Figure 1.7. Virucidal effects observed due to the exposure of FCV coated stainless steel discs to different gas streams at a net gas flow rate of 5 SLM along with the reactive nitrogen species in the liquid phase that covers the virus particles. Details of the treatment conditions have been mentioned in table 1.6. The detection limit of the method for the analysis of virus titer is indicated by a dashed line in figure 1.7(a).

residence time of the species in the mixing chamber and the enclosure tube is ~6.8 seconds until it reaches the virus samples. This correlation between residence time and axial location is used to determine the concentration of species at the location of the samples and reported in table 1.4. The concentration of NO_2 reduces from an initial concentration of 6.1×10^{21} m^{-3} at the beginning of the reactor to below 10^{20} m^{-3} at the location of the virus samples as it reacts with O_3 to form N_2O_5. The calculated $[N_2O_5]$ at the position of the virus sample is 3.0×10^{21} m^{-3}.

Figure 1.8(b) shows the evolution of chemical species in the discharge effluent of the 2D DBD air plasma operating at a discharge power of 14.5 W. Based on modeling of the chemical species arising from a microdischarge in ambient air [34], it is assumed that the plasma only generates NO and O_3 initially on a timescale of 100 μs. The initial values of NO and O_3 have been fixed by ensuring that the measured [O_3] and [NO_2] at the position of the samples is identical to the model concentration at (t = 6.8 s). The residence time of the effluent in the flow-through reactor at the point where O_3 was measured using absorption spectroscopy was 786 ms, while the residence time of the gas analyzer used for NO_x measurement was ~4.24 s (indicated by dashed lines in figure 1.8(b)).

The calculated N_2O_5 concentration at the virus samples for the plasma case and the (O_3+NO_2 – III) case are 1.4×10^{21} m^{-3} and 3.0×10^{21} m^{-3}, respectively. From the positive control tests, it is also seen that [N_2O_5] on the order of 10^{20} m^{-3} leads to significantly smaller inactivation of the FCV samples. In conclusion, [N_2O_5] correlates well with virus inactivation. Unfortunately, N_2O_5 liquid-phase chemistry is not well studied.

In a study investigating the transport of N_2O_5 from the plasma effluent to the liquid phase [41], it was proposed that N_2O_5 is the major source of NO_3^- production in the liquid phase through the following reactions:

$$N_2O_{5_{gas}} \rightarrow N_2O_{5_{aq}}$$

$$N_2O_{5_{aq}} \leftrightarrow NO^+_{2_{aq}} + NO^-_{3_{aq}}$$

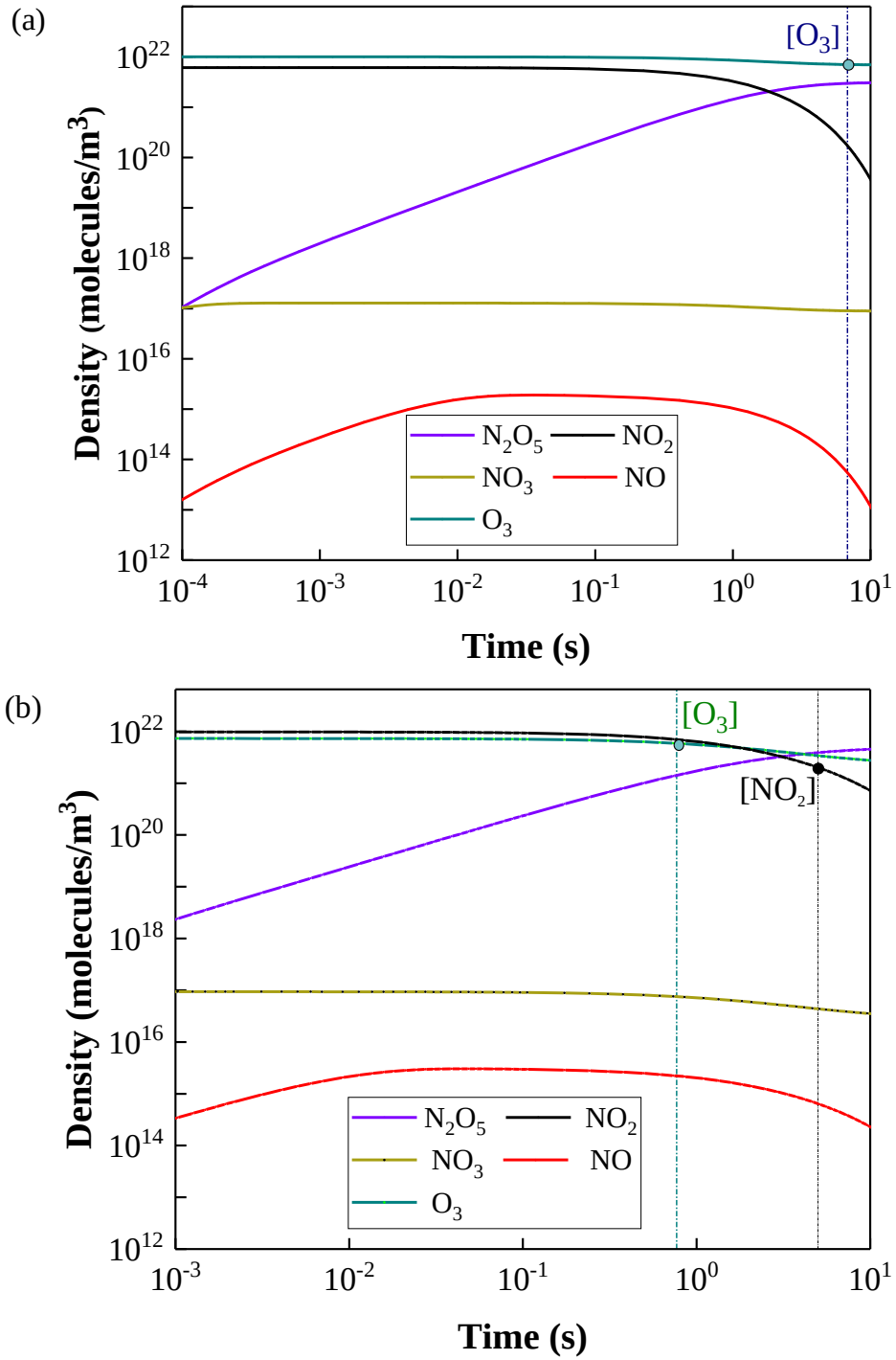

Figure 1.8. Temporal evolution of the species concentrations in the (a) Positive control tests with initial concentrations: $[O_3]_i = 10^{22}$ molecules/m^3, $[NO_2]_i = 6.1\times10^{21}$ molecules/m^3, and (b) Plasma effluent of the 2D DBD. The dashed line in figure 1.8(a) represents the gas residence time at the location of the samples where [O3] was measured. The dashed lines in figure 1.8(b) represent the gas residence times at the points of measurement of $[O_3]$ and $[NO_2]$.

However, NO_3^- does not possess virucidal properties. Despite the negligible quantities of H_2O_2 in the liquid phase due to the absence of humidity in the feed gas, the intermediate species $NO_{2,aq}^+$ could react with $H_2O_{2,aq}$ to give $HOONO_{2,aq}$ (peroxynitric acid) [42] with bactericidal properties [43].

$$NO_{2\,aq}^+ + H_2O_{2\,aq} \leftrightarrow HOONO_{2\,aq} + H^+$$

With analogy to gas-phase chemistry, N_2O_5 can react with H_2O to form HOONO (peroxynitrous acid), which is also virucidal [44]. N_2O_5 could either react with the gas-phase H_2O due to the evaporation of the water droplet or could dissolve in the liquid phase to result in the generation of peroxynitrous acid.

$$N_2O_5 + H_2O \leftrightarrow 2\,HOONO$$

The generation of reactive nitrogen species in the liquid phase is also enhanced by the generation of gas-phase N_2O_5 compared to gas-phase NO_2 because of the two orders of magnitude higher Henry's law constant of N_2O_5 compared to the Henry's law constant of NO_2 [40]. In the case of NO_2, solvation of NO_2 leads to the production of NO^-_2 and NO^-_3. NO^-_2 is not highly virucidal even for a concentration of 3 mM [44]. However, also in this case, the presence of H_2O_2 leads to the formation of peroxynitrous acid which strongly enhances the virucidal effect [44].

1.6. Conclusion

In this work, we compared the effectiveness of surface decontamination by four different plasmas operating in air at atmospheric pressure. We used FCV (a surrogate of human

norovirus) and Salmonella as pathogens. Both plasma sources enabling direct or remote treatment were investigated. It was found that surface humidity significantly enhances the effectiveness of all four plasma-based decontamination approaches. The abundance of reactive species at the position of the pathogen samples in case of direct treatment leads to considerable inactivation of dry samples and much faster inactivation of wet samples than for remote plasma treatment. The remote plasma sources, operated in a flow-through reactor, were notably ineffective against dry samples. The remote DBDs operating at 14.5 W achieved significant inactivation (>4 $\log_{10}$) of wet FCV samples within 4 minutes while the gliding arc discharge at 70 W shows similar effects within 10 minutes. Inactivation with the gliding arc required operation at a higher discharge power. The main species for the gliding arcs were NO and the reduced inactivation in spite of high concentrations of NO is most likely due to the low Henry's law constant of NO compared to NO_2, one of the dominant RNS for the DBD sources. The afterglow of the remote DBDs consist of O_3 and NO_2 that work together towards inactivation of pathogens. Positive control tests with individual gas streams of O_3 and NO_2 lead to very negligible inactivation while a combination of O_3 and NO_2 for the same concentrations obtained complete inactivation. A kinetic model used to study the interaction between the reactive species in the effluent shows a strong correlation between the gas-phase concentration of N_2O_5 with the observed inactivation effects. The calculations suggest that an N_2O_5 concentration of ~10^{21} m^{-3} is highly effective for FCV inactivation.

Chapter 2. Influence of humidity on the efficacy of remote plasma decontamination

2.1. Introduction

Cold plasmas are being widely studied for their potential application towards non-thermal decontamination [10], [21], [45]–[47]. This is due to their capability to induce high chemical reactivity close to room temperature, making them appropriate for the treatment of heat-sensitive substrates. Plasma sources in different configurations have been used in previous studies for the decontamination of food and food-contact surfaces from microorganisms. Foodborne illnesses, caused by enteric viruses such as human norovirus, pose major threats to public health due to outbreaks of diseases such as acute gastroenteritis, mainly through consumption of contaminated agricultural produce [5][6]. A few non-thermal processing technologies have exhibited considerable virucidal efficiencies but they face serious limitations [48][49][50]. Plasma treatments have shown significant virucidal effects against, feline calicivirus, a surrogate for human norovirus [51][52] and are intensively investigated as a possible non-thermal technology for food decontamination.

Plasma treatment setups can be classified as direct or remote based on the method of delivery of the reactive species to the substrate. For a plasma setup performing a direct treatment, the plasma is in direct contact with the substrate being treated and the substrate becomes an integral part of the electrical circuit. In a remote plasma treatment setup, as

used in this work, the discharge is generated at a location that is away from the substrate. Hence, the discharge is not influenced by the physical nature of the substrate which is advantageous for applications.

Nonetheless, the gas residence time is typically longer than the lifetime of the short-lived species for indirect treatments and, it is essential that the reactive oxygen and nitrogen species are controllably administered to the biological substrate for effective decontamination. In addition, the effectiveness of remote plasma-based disinfection has been reported to be strongly dependent on the presence of water on the surface of the substrate [13], [21]. Fridman *et al.* [13] treated samples of *E. Coli* in dry, moist (thin layer of water), and wet (thick layer of water) conditions and observed that the plasma treatment is most effective when the bacteria are covered with a thin layer of water. The efficacy of decontamination decreased for a thicker layer of water, while the observed decontamination was still superior to that of dry samples. Hence, a better understanding of the effect of water and gas-phase humidity on the transport of reactive species from the gaseous plasma effluent to the liquid layer on the substrate is of primary importance to design effective plasma decontamination systems.

This chapter reports a study of the influence of introducing water to the plasma decontamination system by either humidifying the surface of the biological substrates or humidifying the gas fed through the plasma source. The influence of the amount of liquid covering the substrate was investigated through quantification of the reactive species in the liquid layer. Section 2.2 describes the methods involved in virus sample preparation and

its analysis, the plasma source used for the disinfection experiments, the conditions for positive control tests, and techniques for the measurement of the reactive species in the liquid layer. The experimental results are presented in Section 2.3 followed by the key conclusions in section 2.4.

2.2. Experimental Setup and Methods

2.2.1. Pathogen sample preparation and treatment

2.2.1.a Virus assay preparation and titration

Aliquots of the pathogens were applied aseptically on the surface of sterile stainless steel discs. Plasma treatment of the pathogen samples was performed in triplicates, and the averaged results were presented along with the associated uncertainty (standard deviation).

Feline calicivirus (strain 255) was grown and titrated in Crandall-Reese feline kidney (CRFK) cells. The infected mammalian cells were frozen and thawed thrice, and then centrifuged to remove the supernatant. The details regarding the propagation of the virus can be found in [53].

For the experiments, a stock FCV suspension with ~9 $\log_{10}$ $TCID_{50}$/0.1 ml was diluted in sterile distilled water to ~5 $\log_{10}$ $TCID_{50}$/0.1 ml of eluent. Stainless steel discs with a diameter of 11.4 mm were sterilized and placed in the wells of a 24-well microtiter plate. One surface of each disc was spiked with 15 µl of FCV and stored for over 30 minutes under air flow in a biosafety cabinet to allow drying.

After the plasma treatment (see further), the metal discs were recovered in sterile dilution tubes with 1 ml of Phosphate Buffered Solution (PBS). The tubes were vortexed for at least 30 seconds to disperse all virus from the disc into the solution. In brief, serial 10-fold dilutions of eluates were inoculated in CRFK cell monolayers contained in 96-well microtiter plates using three wells per sample. The plate was incubated at 37 ^{o}C, 5% CO_2, and 85% relative humidity and examined for the development of cytopathic effects after about five days. The Kärber method [30] was used for the determination of virus titer which was expressed as 50% tissue culture infective dose per 100 µl of the eluent (log_{10} $TCID_{50}$/100 µl of eluent).

2.2.1.b Bacterial sample preparation and analysis

Salmonella Heidelberg (strain NS-029) was isolated from a chicken breeder farm and used for the experiments [31]. The reader is referred to section 1.2 for further details on the sample preparation process and analysis.

2.2.1.c Pathogen sample treatment

The samples were treated in dry and wet surface conditions. For treatment of wet samples, the surface of the metal discs spiked with the virus were humidified in two different ways prior to exposure to the plasma. With the first approach, a bottle with size-adjustable nozzles was used to spray a volume of 20±5 µl of DI water onto the surface of the discs. The atomized water droplets incident on the metal surface coalesce to form a thin layer of liquid coating the entire surface. To ensure that the surface does not dry out, water was

sprayed every two minutes for treatment times longer than two minutes. In the second approach, a droplet of 40 µl of DI water was pipetted onto the surface of the metal disc, leading to a smaller surface-to-volume ratio when compared to the water layer on the spray sample.

2.2.2. Plasma source

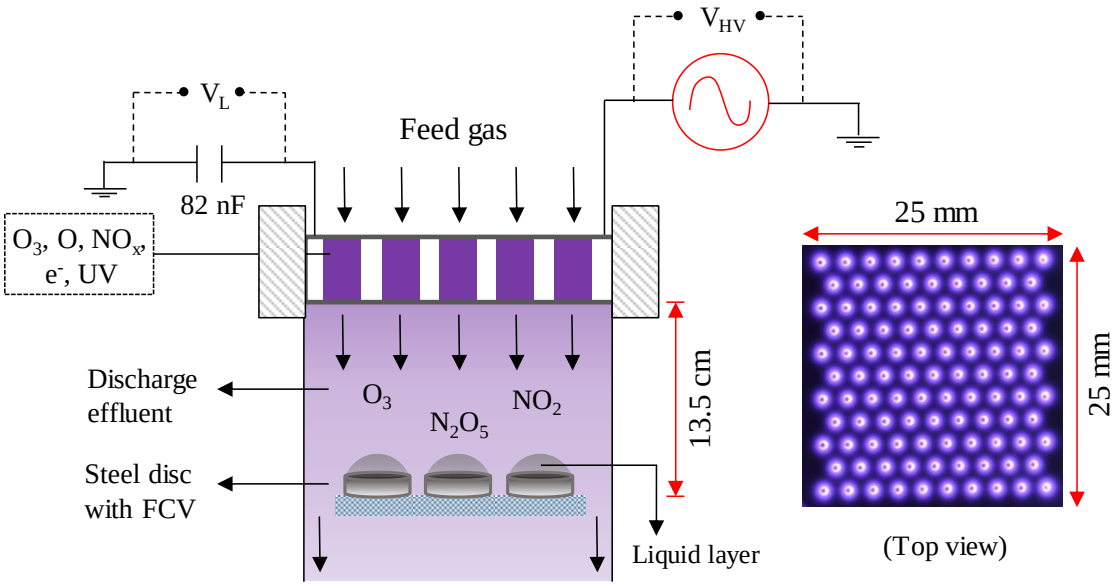

Figure 2.1: Schematic of the experimental setup of the plasma source operating at a discharge power of 14.5 W with either dry air or humid air as the feed gas. For treatment of wet samples, the surface of the metal disc was humidified by spraying DI water of (20±5) µl or by pipetting a droplet of DI water of 40 µl onto the surface.

A dielectric barrier discharge was operated at a constant discharge power of 14.5 W. Figure 2.1 shows the schematic of the plasma source used in this work including the treatment configuration of the FCV samples. This DBD consisted of an array of 105 holes with a diameter of 600 µm and a thickness of 500 µm within which micro-discharges were generated. The plasma source was operated in dry or humid air at a constant gas flow rate

of 16.4 SLM which corresponds to a gas residence time of 164 μs in the discharge region. The reader is referred to [19] for more detailed information about the plasma source.

To generate a discharge in the absence of humidity, dry air at a flow rate of 16.4 SLM was delivered to the plasma source through a mass flow controller (MKS GE50, MKS Instruments Inc., USA). To humidify the air, the dry air supply was split equally into two mass flow controllers connected in parallel and then routed through two gas washing bottles to reduce the gas flow rate through the washing bottles. The exit gas streams of the two bottles were merged and delivered to the plasma source.

To reduce radial losses of the chemical species from the plasma effluent to the ambient air, a polycarbonate tube of diameter 52 mm was attached at the bottom. Three pathogen samples were placed on a 30×30 mm teflon block within the cylindrical enclosure at a distance of 13.5 cm from the plasma. The plasma-generated long-lived reactive species were blown onto the samples for a one-time interaction before they were routed to the exhaust.

To identify the gas-phase species leading to inactivation, the concentrations of O_3 and NO_x generated by the plasma were measured in the effluent using UV absorption spectroscopy and a gas analyzer (ENERAC 500, ENERAC), respectively. The measurements were performed at the location of the biological samples. The reader is referred to section 1.2.4 for further details.

2.2.3. Positive control tests

To study the gas-to-liquid phase transport limitations encountered by the reactive species, FCV samples were exposed to different positive controls. The samples were treated in both droplet and water spray surface conditions. A gas flow with O_3 at a concentration of 363 ppm, equal to the concentration of O_3 in the air plasma, was generated by an Ar/O_2 plasma in the 2D DBD. Gas flows containing 500 ppm of NO_2 or NO were obtained from gas bottles containing 500 ppm NO_2/N_2 and 1000 ppm NO/N_2, respectively. For lower concentrations of NO_2 and NO, the gas flows from the bottles were diluted with Ar. All positive control measurements were performed at a constant flow rate of 16.4 SLM.

Further positive control tests were performed with NO_2, and mixtures of NO_2 and O_3 at a total gas flow rate of 5 SLM to produce N_2O_5. The details of the procedure can be found in section 1.3. The initial concentrations of O_3 and NO_2 were measured at the beginning of the reactor before any gas-mixing occurs by techniques mentioned in section 1.2.4. The concentrations of O_3, NO_2, and N_2O_5 at the location of the sample were calculated using the kinetic model described in section 1.4. The modeling results are consistent with the experimental measurement of $[O_3]$ at the location of the samples.

2.2.4. Liquid droplet size measurement

The thickness of the water layer covering the virus sample has a strong influence on the transport of reactive species into the liquid layer. The exposure of the wet sample to the plasma effluent or even the gas flow leads to evaporation of the water droplet. The amount of evaporation of the water droplets was quantified when the samples were exposed to dry

and humid air, with and without the discharge ignited, for a period of 5 minutes. This was done by measuring the weights of the samples before and after the treatment using an analytical balance (Sartorius Entris 124-1S). Droplets with a volume of 10, 20, 30, and 40 μl were placed on the discs and exposed to a gas flow and to the plasma effluent, both at the same flow rate of 16.4 SLM with the discharge operating at 14.5 W. The thickness of the droplet was measured by analyzing photographs of the samples taken using a digital camera (Nikon D3100). Image processing was performed on the photographs to measure the volume of the residual water layer, and the results were in agreement with the calculations performed using the weights of the samples.

2.2.5. Reactive nitrogen species in the liquid layer

The reactive nitrogen species in the liquid layer were quantified using absorption spectroscopy based on the Griess assay as described in [54]. The Griess reagent was prepared by mixing equal volumes of N-(1-naphthyl) ethylenediamine dihydrochloride (0.1% (1 $mg \cdot ml^{-1}$) solution) and sulfanilic acid (1% (10 $mg \cdot ml^{-1}$) solution in 5% phosphoric acid) present in the Griess Reagent Kit (G-7921, Molecular Probes). Vanadium (III) Chloride, prepared by adding 400 mg of solid VCl_3 to 50 ml of 1M HCl, was used for the reduction of nitrates to nitrites in the solution. Multiple samples were treated simultaneously and 100 μl was extracted from the treated samples with a pipette and added to a 96-well microtiter plate. 10 μl of a buffered solution (pH 8±0.2) was added immediately after treatment to stop the conversion of nitrites into nitrates in an acidic medium. The addition of the buffer, however, does not prevent the conversion of nitrites

into nitrates due to oxidation by ozone. 10 µl of sodium pyruvate was added to scavenge H_2O_2 as it might affect the Griess assay. 80 µl of either DI water or VCl_3 solution (for converting nitrates to nitrites) was added to the sample after the addition of 20 µl of Griess reagent for the quantification of the nitrite and total nitrite/nitrate concentrations, respectively. The concentrations of nitrates were obtained by taking the difference between the measured total nitrite/nitrate concentration and the measured nitrite concentrations.

A photometric reference sample (control) was prepared by following the same protocol but using 100 µl of DI water instead of plasma-treated samples. After 30 minutes of incubation of the nitrite samples at room temperature and the nitrate samples at 37 ^{o}C, the samples were transferred into a micro-cuvette and the absorbance was measured at 565 nm using a broadband spectrometer (Avantes AvaSpec-2048) and an LED (M565L3, Thorlabs) as light source. The absorbance was calibrated with known concentrations of sodium nitrite solutions from 10-100 µM. For analysis of samples with higher nitrite concentrations, the samples were diluted with DI water so that the absorbance fell within the range of calibration and no saturation of absorbance occurred.

The NO_2^- and NO_3^- concentrations were measured in droplets of varying sizes when treated with the dry air plasma for 30 seconds. The positive control treatments were also performed for a duration of 30 seconds on droplets of 40 µl for measurement of the same species. Concentrations of these species were also determined as a function of time when a droplet of 40 µl was treated by the effluent from the discharge at 14.5 W generated with dry air and humid air as the feed gas.

2.2.6. Hydrogen peroxide in the liquid layer

Using the colorimetric method [55], the concentration of H_2O_2 in the liquid was measured when a droplet of 40 µl was treated with the plasma operating at a power of 14.5 W with dry air and humid air as the feed gas. 13.3 µl of 10 mM NaN_3 was added to a 96-well microtiter plate. 100 µl of the sample was added to the azide solution immediately after plasma treatment to quench the reactive nitrogen species that could react with H_2O_2. Then, 100 µl of titanium oxysulphate ($TiOSO_4$) solution was added. The solution was transferred into a micro-cuvette and the absorbance was measured at 405 nm using a broadband spectrometer (Avantes Avaspec-2048) and an LED (M405LP1, Thorlabs) as the light source.

2.3. Results and Discussion

2.3.1. Influence of humidity on the effectiveness of disinfection

Figure 2.2 shows the residual FCV and *Salmonella Heidelberg* titers after exposure to the plasma effluent as a function of time. The results demonstrate that the efficacy of plasma treatment is strongly dependent on the surface humidity of the pathogen samples. The negligible inactivation observed when a dry sample was treated is consistent with reports in the literature that suggest the requirement for the presence of water for disinfection using plasma and ozone [21][37][38]. The presence of water might enhance oxidation of the capsid proteins similar to enhanced lipid peroxidation rates in the presence of water [39], [56]. Complete inactivation of FCV and Salmonella for dry air treatment take about 4

minutes and 5 minutes, respectively. Exposure of the pathogens to plasma generated in humid air requires similar time for complete inactivation in spite of lower initial bacteria titer in case of humid air plasma. The longer treatment time required for inactivation of Salmonella suggests that FCV is more susceptible to the plasma-generated species than Salmonella.

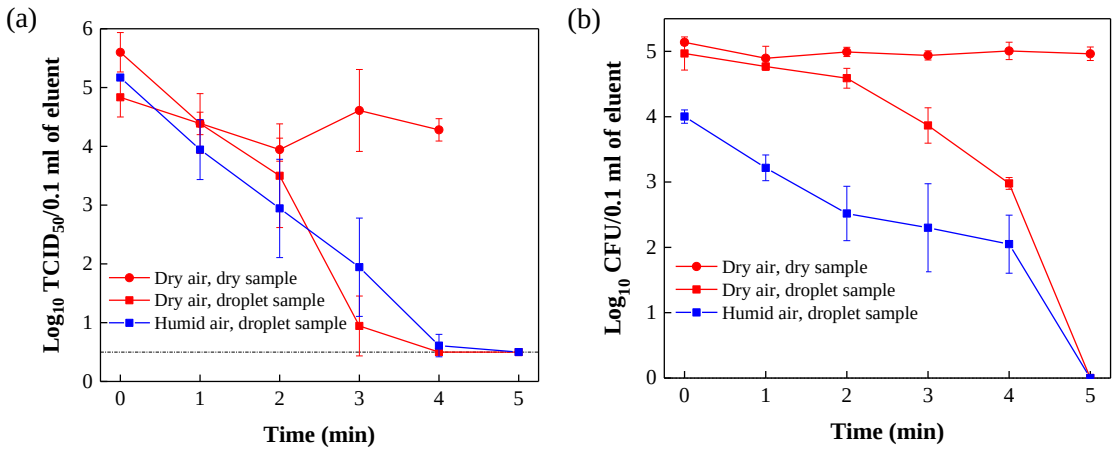

Figure 2.2. Antimicrobial effects induced by the 2D DBD on (a) FCV, and (b) Salmonella samples as a function of treatment time. The plasma source was operated at a discharge power of 14.5 W with dry air and humid air as the feed gas. For the treatment of wet samples, a droplet of 40 µl was pipetted on to the surface of the metal disc. The detection limit of the method for analysis of virus titer is indicated by a dashed line.

Figure 2.3 shows the effect of plasma treatment when the metal discs spiked with FCV were treated in different surfaces conditions. While the plasma treatment of the dry sample leads to less than 1 $\log_{10}$ inactivation within 4 min, the spray and droplet samples take 3 and 4 minutes for complete inactivation of the virus, respectively. The differences in the effectiveness of plasma treatment for the spray and droplet samples might be due to the transport limitations of the gas-phase reactive species into the liquid phase before reaching the virus.

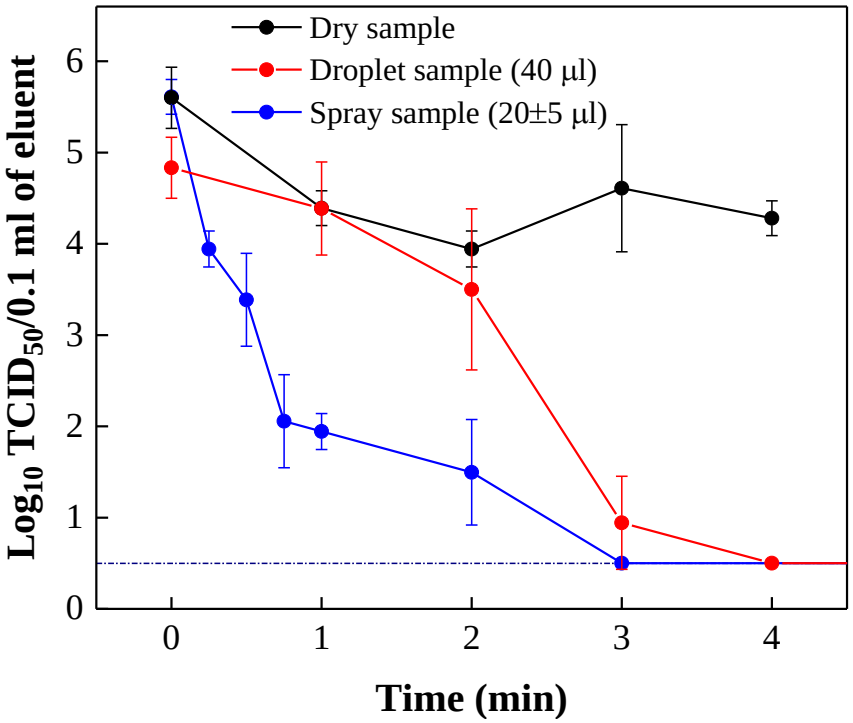

Figure 2.3. Virucidal activity of the 2D DBD as a function of treatment time. The 2D DBD operated at a discharge power of 14.5 W with dry air as the feed gas. The plasma effluent was used to treat samples in dry and wet conditions. For the treatment of wet samples, the surface was humidified by either pipetting a water droplet of volume 40 µl or spraying water of volume 20±5 µl. The detection limit of the method for analysis of the virus titer is indicated by a dashed line in figure 2.3.

The treatment conditions of figure 2.4 are given in table 2.1. Figure 2.4(a) shows the treatment of FCV samples with O_3, NO_2 and NO for a 40 µl droplet and for water spray of 20±5 µl. Treatment of FCV samples with water spray with gas flows containing O_3 and NO_2 for 5 minutes led to >4 $\log_{10}$ reduction in the virus titer, while only ~1 $\log_{10}$ inactivation of the virus titer was observed in case of droplet samples. This observation points to transport limitations of O_3 and NO_2 from the gas to the liquid phase. Exposure to NO leads to negligible inactivation in both the droplet and spray cases.

Table 2.1. Initial gas-phase concentrations of reactive species and at the location of the FCV samples for conditions utilized for the treatment of wet FCV samples. The results of the treatment are shown in figures 2.4(a) and 2.4(b). [NO_2] for the mixing conditions and [N_2O_5] have been estimated from the model at the location of the samples.

	Initial concentrations (m^{-3})		**Concentrations at the sample (m^{-3})**		
Treatment condition	**[O_3]**	**[NO_2]**	**[O_3]**	**[NO_2]**	**[N_2O_5]**
Air plasma (14.5 W)	7.3×10^{21}	9.8×10^{21}	3.5×10^{21}	2.1×10^{21}	1.4×10^{21}
O_3 – I	8.9×10^{21}	-	8.9×10^{21}	-	-
NO_2 – I	1.2×10^{22}	-	-	1.2×10^{22}	-
O_3 – II	10^{22}	-	10^{22}	-	-
NO_2 – II	-	6.1×10^{21}	-	6.1×10^{21}	-
$O_3 + NO_2$ – I	10^{22}	7.5×10^{20}	9.6×10^{21}	4.7×10^{17}	3.7×10^{20}
$O_3 + NO_2$ – II	10^{22}	1.5×10^{21}	9.3×10^{21}	1.2×10^{18}	7.4×10^{20}
$O_3 + NO_2$ - III	10^{22}	6.1×10^{21}	7.0×10^{21}	2.1×10^{19}	3.0×10^{21}

Figure 2.4(b) shows the virucidal effects induced when wet virus samples were treated by O_3, NO_2, and mixtures of O_3 and NO_2. Exposure to a combination of O_3 and NO_2 enables full inactivation for the highest concentrations of O_3 and NO_2 used for both droplet and spray FCV samples while the FCV inactivation of droplet samples is negligible after exposure to individual streams of O_3 and NO_2 at the same concentrations within the experimental uncertainty and less than 2 $\log_{10}$ for spray samples. An analysis of the reactive

nitrogen species in the liquid layer and a discussion of these results in the context of gas-to-liquid transport limitations are provided later.

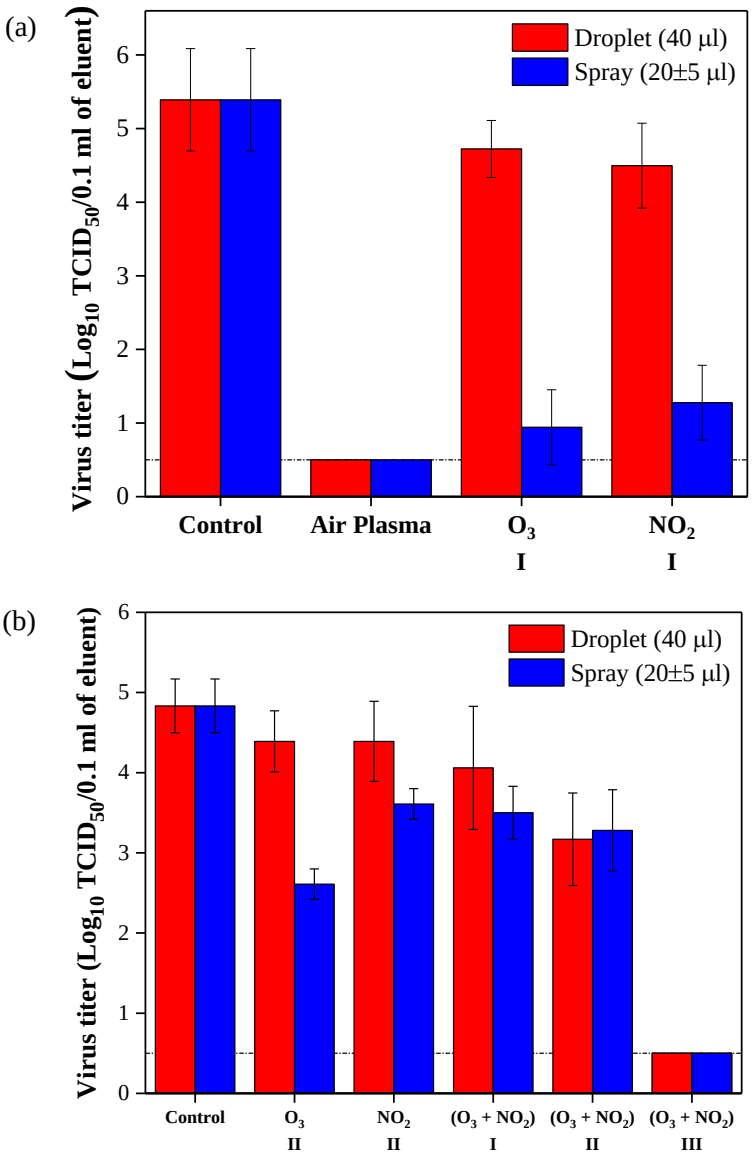

Figure 2.4. Inactivation of wet FCV samples after exposure to different treatment conditions for 5 minutes. The figure illustrates the influence of the method of surface humidification on the efficacy of plasma treatment. The species concentrations to which the samples were exposed are shown in table 2.1. FCV samples were exposed to the effluent at a net flow rate of: (a) 16.4 SLM, and (b) 5 SLM. The detection limit of the method for analysis of the virus titer is indicated by a dashed line.

2.3.2. Evaporation and reactive species concentrations in the liquid layer

Treatment time (min)	Flow-control	Plasma-treated
0		
2		
5		

Figure 2.5. Photographs of the droplet on a sample during treatment with dry air at a flow rate of 16.4 SLM in the absence (flow-control) and presence of plasma. The initial droplet volume (t=0) is 40 µl. Additionally, the droplets after 2 and 5 minutes exposure are also shown.

The exposure of wet samples to the gas flow and the plasma effluent leads to evaporation of the liquid layer. Figure 2.5 shows images of a 40 µl droplet exposed to a flow rate of 16.4 SLM. The images were taken for the flow-control (with no discharge) and in the presence of a discharge. Figure 2.6 shows the volume loss relative to the initial droplet volume for different droplet volumes when the substrates were treated for a duration of 5 minutes. The amount of evaporation is higher when the discharge is generated compared to the flow-control due to increase in gas temperature by the plasma. Also, the amount of evaporated liquid is higher when the samples were exposed to dry air than when they were exposed to humid air. Considerable evaporation was noted, however, even with exposure to humid air, denoting that the relative humidity of the feed gas was actually lower than 100%. This could be due to incomplete saturation of the gas when going through the bubbler due to the large gas flow rate or cooling down of the liquid in the bubbler. A larger

amount of evaporation of the liquid layer leads to a smaller surface to volume ratio, impacting the transport of reactive species into the liquid during the treatment. It also increases the H_2O concentration in the gas-phase, with possible impact on the chemical composition of the plasma effluent in the immediate vicinity of the droplet sample.

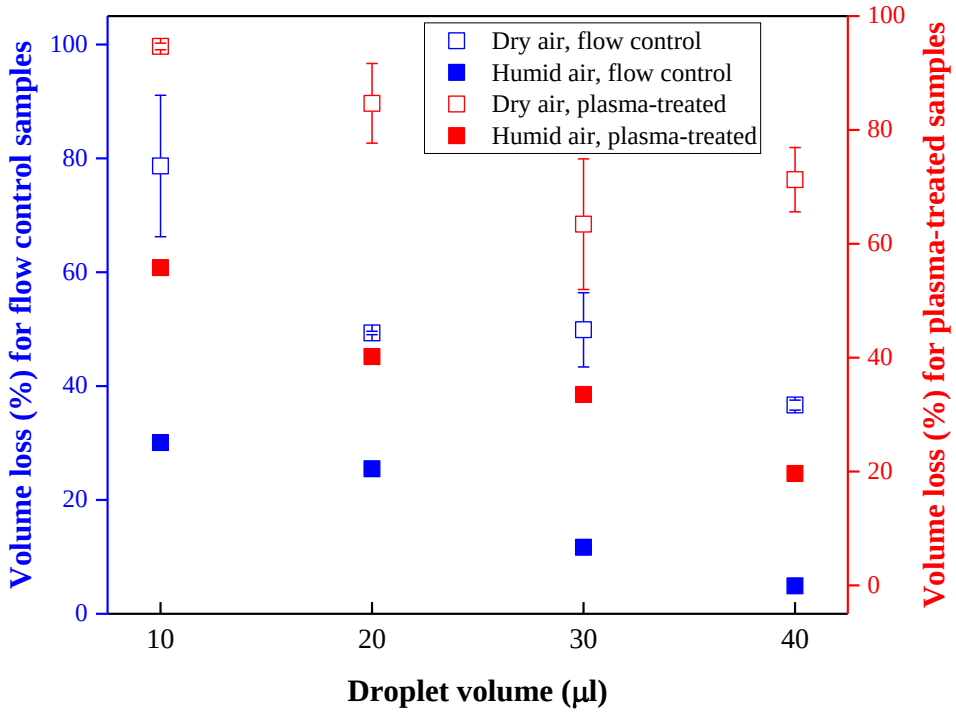

Figure 2.6. Volume loss (%) for samples with droplets of different volumes on the surface when treated with the feed gas at a flow rate of 16.4 SLM in the absence (flow-control) and presence of plasma. Dry and humid air have been used as feed gas.

Figure 2.7 shows the concentration of nitrites and nitrates in the liquid layer when samples with different amounts of water were treated with the dry air plasma at 14.5 W. It is seen that the concentration of nitrites and nitrates are highest in the spray sample. $NO_{3,aq}^-$ decreases as the droplet volume increases, while the uncertainty of measurement in $NO_{2,aq}^-$ is too large to draw any conclusions from the variation in the measurement of $NO_{2,aq}^-$. The

larger amount of liquid RNS in the spray sample compared to the 40 µl droplet correlates with the faster inactivation encountered with the FCV spray sample compared to the effects against the 40 µl droplet sample (figure 2.3).

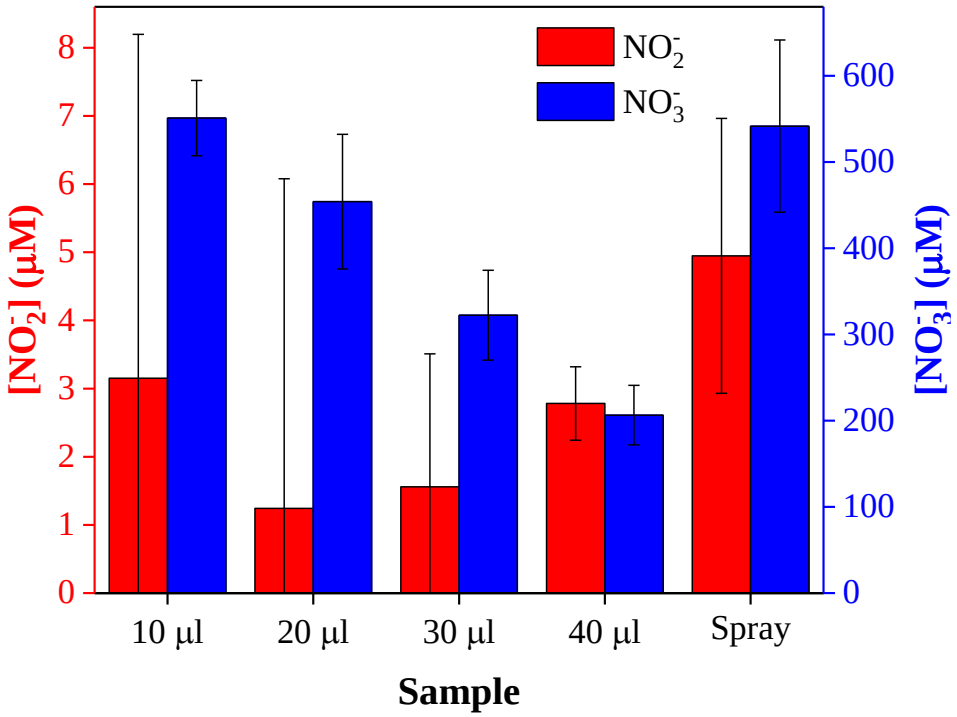

Figure 2.7. Concentrations of NO_2^- and NO_3^- in the liquid phase when samples with different water quantities were exposed to the 2D DBD plasma working at 14.5 W with dry air as the feed gas. The samples were treated for 30 s.

Figure 2.8 shows the concentrations of nitrites and nitrates in the liquid layer when a 40 µl droplet was treated with NO_2, and mixtures of O_3 and NO_2, the concentrations of which have been mentioned in table 2.1. The solvation of NO_2 leads to the production of $NO_{2\,aq}^-$, which is not strongly virucidal for concentrations up to 3 mM [44]. $NO_{2\,aq}^-$ reaches a concentration of only 50 µM for a treatment time of 30 seconds, and hence negligible virucidal effects were observed (see figure 2.4(b)). For conditions with mixtures of O_3 and

NO_2, however, very negligible concentrations (<10 µM) of $NO_{2\,aq}^-$ were detected in the droplet. This is most likely due to the fast oxidation of the produced NO_2^- by $O_{3,aq}$ or a reduced production of NO_2^- due to a reduction in gas-phase NO_2 in favor of N_2O_5 (see also further). The larger Henry's law constant of N_2O_5 compared to the Henry's law constant of NO_2 (~170 times) leads to much better transport of RNS into the liquid phase [40]. It must be noted that NO_3^- does not exhibit any virucidal properties.

$$NO_{2,aq}^- + O_{3,aq} \rightarrow NO_{3,aq}^-$$

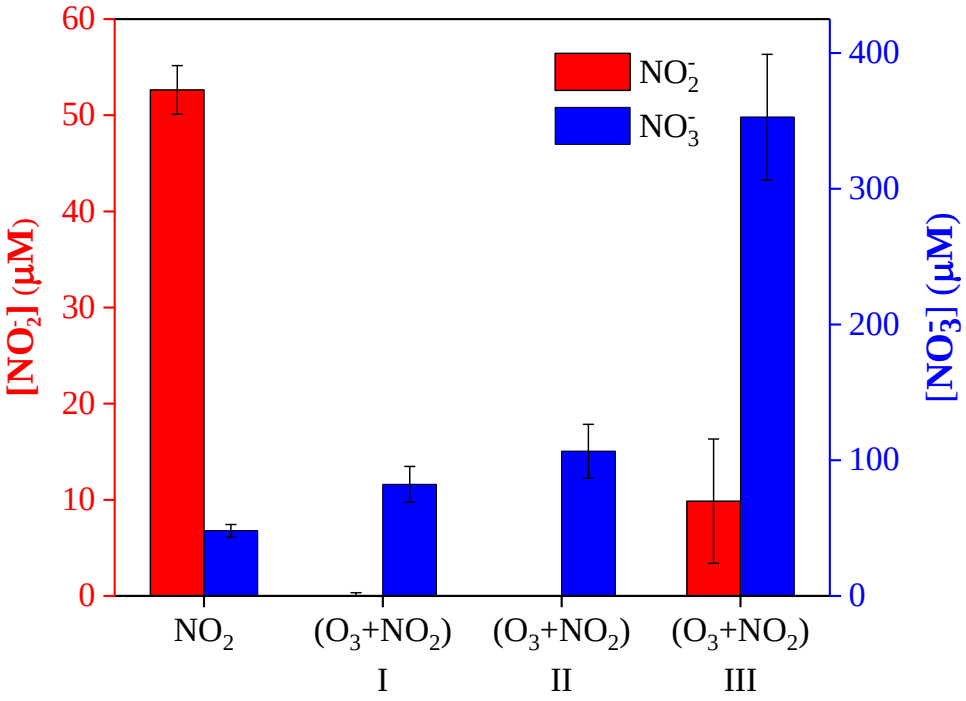

Figure 2.8. Concentrations of NO_2^- and NO_3^- in the liquid phase when a sample with 40 µl droplet was exposed to different streams at a net gas flow rate of 5 SLM. The gas phase species concentrations are reported in table 2.1.

In the gas phase, N_2O_5 could react with water to give peroxynitrous acid [57] or nitric acid [58] in two competing reactions. These reaction rate coefficients of both these reactions are of the order ~10^{-27} $m^3 \cdot s^{-1}$. These reactions could occur with the evaporated water from the droplet or an equivalent reaction could occur in the liquid phase after the solvation of N_2O_5 in the liquid layer.

$$N_2O_5 + H_2O \rightarrow 2\,HNO_3$$
$$N_2O_5 + H_2O \rightarrow 2\,HOONO$$

In view of the large concentration of NO_3^- in the mixture case, it is highly likely that a significant concentration of ONOOH is generated as well. While peroxynitrous acid is strongly virucidal [44], nitric acid, however, does not possess any virucidal attributes.

Table 2.1 reports the calculated concentrations of N_2O_5 in the gas-phase for each of the mixture conditions, and it is seen that the N_2O_5 generated with mixing of the highest concentration of NO_2 with O_3 leads to complete inactivation of FCV in both droplet and spray samples. The gas-phase [N_2O_5] corresponding to this case in the droplet sample is 3×10^{21} m^{-3}. The larger Henry's law constant of N_2O_5 compared to O_3 and NO_2 could be a possible explanation for insignificant differences in virus inactivation between the droplet and spray samples unlike the case of O_3 and NO_2 because the interfacial gas-liquid transfer of N_2O_5 is not transport-limited.

Figures 2.9(a) and 2.9(b) show the nitrites, nitrates, and hydrogen peroxide concentration in the liquid phase when a 40 µl droplet was treated with plasma at 14.5 W generated with

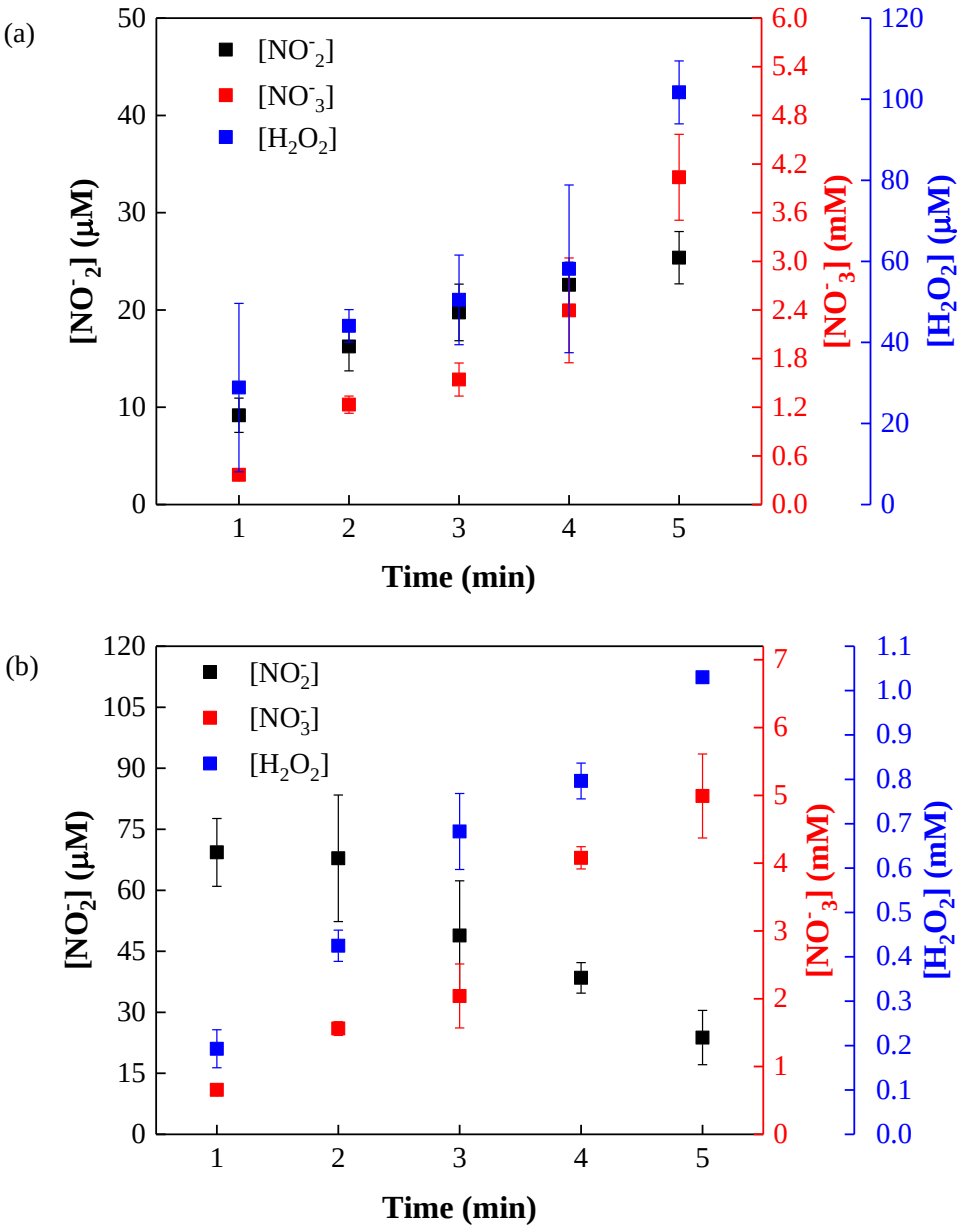

Figure 2.9. Concentrations of NO_2^- and NO_3^- in the liquid phase when a sample with 40 µl droplet when exposed to the plasma generated at a discharge power of 14.5 W with: (a) Dry air, and (b) Humid air as feed gas. The gas flow rate was kept constant at 16.4 SLM.

dry air and humid air as feed gas, respectively. At the location of the samples, gas-phase O_3 remained constant at 3.5×10^{21} m^{-3} and 2.1×10^{21} m^{-3} in the dry air and humid air plasma

cases, respectively. It has been shown that up to 5 mM of [H_2O_2] in the liquid-phase leads to insignificant inactivation of FCV titer [44]. The presence of H_2O_2 and NO_2^-, however, can also lead to the generation of peroxynitrous acid [59] with strong virucidal properties [44], which is a prominent reaction in case of plasma treatment with the discharge generated in humid air.

$$NO_2^- + H_2O_2 + H^+ \leftrightarrow 2\ HOONO + H_2O$$

The concentration of H_2O is 5 orders of magnitude higher than the concentration of H_2O_2 in the droplets, and hence the reaction between N_2O_5 and H_2O might indeed be the dominant pathway towards the generation of peroxynitrous acid, at least if the rate coefficients are not largely different. It is evident from the kinetic model (section 1.4) that the generation of gas-phase N_2O_5 is strongly dependent on the concentration of O_3 in the plasma effluent. The lower O_3 concentration at the sample location in case of the humid air plasma implies a lower concentration of gas-phase N_2O_5, which results in a decreased generation of peroxynitrous acid through this pathway. Nonetheless, the presence of a significant concentration of H_2O_2 (~1mM) in liquid layer treated by the plasma generated in humid air boosts the generation of peroxynitrous acid.

2.4. Conclusion

In this work, the influence of liquid layer on the substrate has been studied for remote plasma-based decontamination by the 2D DBD, including the effect of dry air and humid air as the feed gas. Dry samples show negligible virus inactivation when treated by the

remote plasma source. Decontamination by O_3 and NO_2 were less effective when the substrate was covered by a thicker layer of water compared to the water spray. This was found with exposure to plasma effluent and a mixture of NO_2 and O_3 producing N_2O_5. Concentrations of reactive nitrogen species in water layers of varying volumes correlate well with the efficacy of plasma treatment. A kinetic model (section 1.4) shows the generation of N_2O_5 in the gas-phase due to synergistic effects arising from the interaction between ozone and nitrogen dioxide in the plasma effluent, the concentration of which correlates well with FCV inactivation. The reaction of N_2O_5 with H_2O most likely results in the simultaneous generation of HNO_3 and HOONO at comparable rates. Treatment of the samples with mixtures of O_3 and NO_2 also results in complete inactivation for the highest concentration of NO_2, and the inactivation trend correlates well with the concentration of $NO_{3,aq}^-$. suggesting the role of peroxynitrous acid in the aqueous phase towards inactivation of FCV. The lower gas-phase concentration of O_3 in case of humid air plasma leads to a lower concentration of gas-phase N_2O_5 and thus results in a lower concentration of peroxynitrous acid through this dominant pathway. This is compensated by the enhanced formation of peroxynitrous acid when nitrites and hydrogen peroxide co-exist in the liquid layer in considerably large quantities for a plasma generated with humid air as the feed gas. This is most likely the cause for similar inactivation of FCV using both dry and humid air plasmas in spite of the expected large differences in the gas-phase RONS as illustrated by the large concentration of H_2O_2 in the droplet, making N_2O_5, H_2O_2, and HNO_2 production in the gas phase important for effective decontamination using plasma. The results suggest that the disinfection capabilities of remote plasmas could be hindered

by the transport limitations encountered by reactive species from the gas to liquid phase, the enhancement of which is essential for the optimization of plasma-based disinfection systems.

Chapter 3. Comparison of plasma sources and UV-C for virus inactivation

3.1. Introduction

Cold atmospheric pressure plasma is a promising technology for non-thermal disinfection amongst other areas of plasma biomedicine. The strong chemical reactivity induced by cold plasmas close to room temperature makes it an appropriate candidate for decontamination of heat-sensitive substrates. There are numerous studies exploring the germicidal activity of cold plasmas against foodborne bacteria, viruses, fungi, and parasites [10]–[12], [16], [21], [27], [46], [60]–[62]. Disinfection using cold plasma can be achieved through interaction of the substrate with either the discharge or the gas treated by the discharge. It was shown that direct contact of the substrate with the plasma causes bacterial inactivation at a much faster rate than in case of remote treatment when the same DBD setup was used for sterilization [10]. Direct discharges could achieve >3 $\log_{10}$ reduction in the number of bacterial cells when used to treat surfaces contaminated with *Pseudomonas Aeruginosa* [12]. Minimal inactivation of human Norovirus (HuNoV) was achieved with treatment of human stool suspensions in water with cold plasma [60]. An RF plasma jet was used to treat feline calicivirus (FCV), a surrogate of HuNoV, in liquid media and the dependence of the virucidal activity on plasma power, exposure distance, feed gas mixture, and virus suspension medium was investigated [16]. We have also identified the primary chemical pathways for disinfection when a two-dimensional array of microdischarges was used to treat surfaces and liquid solutions against FCV [21]. Pavlovich *et al.* used a surface

discharge for disinfection of aqueous solutions of *Escherichia Coli* and correlated the antibacterial effects observed with the estimated ozone concentrations in the solution which is severely limited by gas-to-liquid phase transport [27]. A gliding arc reactor was used to effectively treat different surfaces contaminated with *E. Coli* and *Staphylococcus Epidermidis* [11]. Liao *et al.* provided a review of the processing parameters affecting bactericidal attributes of the plasma and the possible mechanisms leading to disinfection [46].

Previous studies have also investigated disinfection of contaminated fresh produce with considerable success [47], [63]–[69]. Plasma treatment of strawberries and cherry tomatoes inoculated with different bacterial pathogens was performed by placing them in a container between the electrodes with the substrates removed from the discharge [63]. Treatment of Tulane virus, *E. Coli*, and Salmonella inoculated on Romaine lettuce performed in petri dishes and polyethylene pouches using a DBD demonstrated a reduction of ~1 $\log_{10}$ for all the pathogens irrespective of the packaging material [47]. Niemira *et al.* evaluated the dependence of the effectiveness of a gliding arc reactor in disinfecting apples inoculated with *E. Coli* on the gas flow rate through the discharge [64]. Microwave-powered cold plasma operating on nitrogen and helium-oxygen gas mixtures, employed to inactivate *E. Coli* and Salmonella, identified the dependence of inactivation on the pH of the food substrate [65]. An array of plasma jets used to treat fresh produce inoculated with *E. Coli* led to limited inactivation while a high degree of electroporation and disruption of membrane of the damaged bacterial cells was observed [66]. Inactivation was found to be

dependent on the surface of the substrate as the irregularities in the surface may provide a physical barrier to the microorganisms from the plasma [65], [67].

Many other emerging non-thermal technologies have shown notable virucidal efficacies. Ionizing radiation has high disinfection potential and is probably one of the most versatile among non-thermal food preservation technologies. However, its development and commercialization have been hampered by unfavorable public perception [48]. Pulsed light technology, involving the application of short and intense pulses of light in the ultraviolet to near infrared (UV–NIR) range, is also effective in decontaminating foods and food-contact surfaces from foodborne viruses [70], [71]. Nonetheless, poor penetrating power of light requiring transparent and smooth surfaces limits the applicability of pulsed light [48], [72]. High Hydrostatic Pressure (HHP) technology showed considerable effectiveness against foodborne pathogens [49], [73], [74] but it can affect the rheological properties of food products [75]. In addition, it requires sophisticated equipment and is effective only against foods with high acidity [48].

UV-C treatment is a well-established decontamination technology [76]. Numerous studies demonstrate the virucidal attributes of UV-C radiation against pathogens such as hepatitis A virus (HAV), murine norovirus (MNV) and FCV [36], [76]–[79]. This process does not require the addition of chemicals and results in minimal changes in color, flavor, odor, or pH of the treated food. However, the use of UV-C radiation has limitations such as: (i) requirement of close proximity between the source of radiation and the target [50], [80]; (ii) the inability of UV to penetrate opaque materials, thus leading to the shadowing effect

[50], [80]; and most importantly, (iii) the capability of inactivated bacterial pathogens to revive under certain storage conditions through the phenomena of photo-reactivation and dark-repair of the UV-damaged genome [36]. While some viruses carry the genes for repair enzymes [36], most use the repair enzymes of the host cell to repair their genome after undergoing UV treatment.

Although reported results show good virucidal efficacy of cold plasmas, the cost of this emerging technology has to be minimized to be affordable by the food industry. As plasmas produce reactive species through the consumption of electricity, electrical energy consumption is one of the major parameters that determines the operational costs of plasma technology. Unfortunately, most studies reporting decontamination of pathogens by plasmas do not focus on energy consumption.

Enteric viruses, such as human Norovirus, are responsible for outbreaks of foodborne illnesses such as acute gastroenteritis through contamination of fresh produce and minimally processed foods. The estimated global cost of human norovirus is $4.2 billion in the public health system [6], [81]. For the plasma treatment experiments, we use FCV as a surrogate for HuNoV. The similarities in pathological/biological characteristics of HuNoV and FCV have been the reason for the usage of FCV as a surrogate for HuNoV in previous studies [52], [82]. Due to its higher resistance towards chemical disinfectants, the use of FCV as a surrogate to HuNoV is also advocated for initial virucidal effectiveness tests by the US Environmental Protection Agency [51].

In this study, we compare different plasma sources based on dielectric barrier discharge technology in terms of their energy consumption and practical applicability. Two kinds of plasma treatments were conducted: direct treatment in which the plasma is in direct contact with the substrate, and remote treatment in which the plasma effluent containing the reactive species is blown onto the substrate. Most reactors are continuous flow reactors but we also report a batch reactor prototype to explore an example of a higher energy efficiency plasma-based disinfection system. The reported energy costs and virucidal efficacy of the plasma sources are also compared with those of conventional UV disinfection technology and the advantages and disadvantages are assessed.

3.2. Experimental Setup and methods

3.2.1. Plasma sources

Three different DBD plasma sources were used in this study. These plasma sources offer treatment of the pathogens in either direct contact or remote treatment modes, depending on the plasma source configuration and proximity of the discharge to the substrate. Each of the plasma treatment configurations is described below.

(a) 2D array of integrated micro-hollow dielectric barrier discharge (2D DBD)

The 2D DBD setup (figure 3.1) is described in detail in [21]. The source consist of an array of micro-hollow DBDs leading to high power density and large concentrations of reactive oxygen and nitrogen species. This array of microdischarges was housed in a home-made polytetrafluorethylene (PTFE) holder which accommodated the electrical connections and

feed gas delivery. The plasma source was driven by an AC power supply (PVM500) in dry air at a discharge power and frequency of 14.5 W and 20 kHz, respectively. The plasma source was operated with a continuous gas flow rate of 16.4 SLM. To avoid radial losses of the reactive species to the ambient, a polycarbonate tube was fixed downstream of the electrode to serve as an enclosure. Biological samples were placed on a platform within this enclosure at a distance of 13.5 cm from the discharge. The virus samples were not in direct contact with the plasma and were treated by the reactive oxygen and nitrogen species in the discharge effluent. The plasma power was measured by the Lissajous method as described previously in [39]. Applied voltage and voltage across the external capacitor were recorded using a HV probe (Tektronix P6015A, 1000X) and a capacitive probe (Tektronix TPP0200, 10X), respectively.

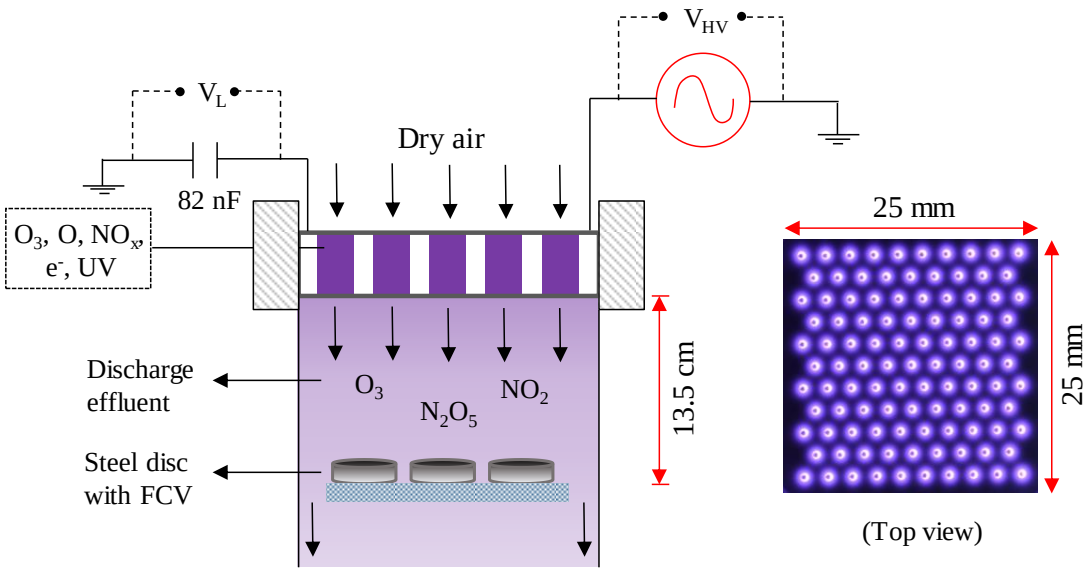

Figure 3.1: Schematic of the 2D DBD used for the treatment of FCV samples. A photograph of the top view of the discharge is shown on the right.

(b) Direct DBD

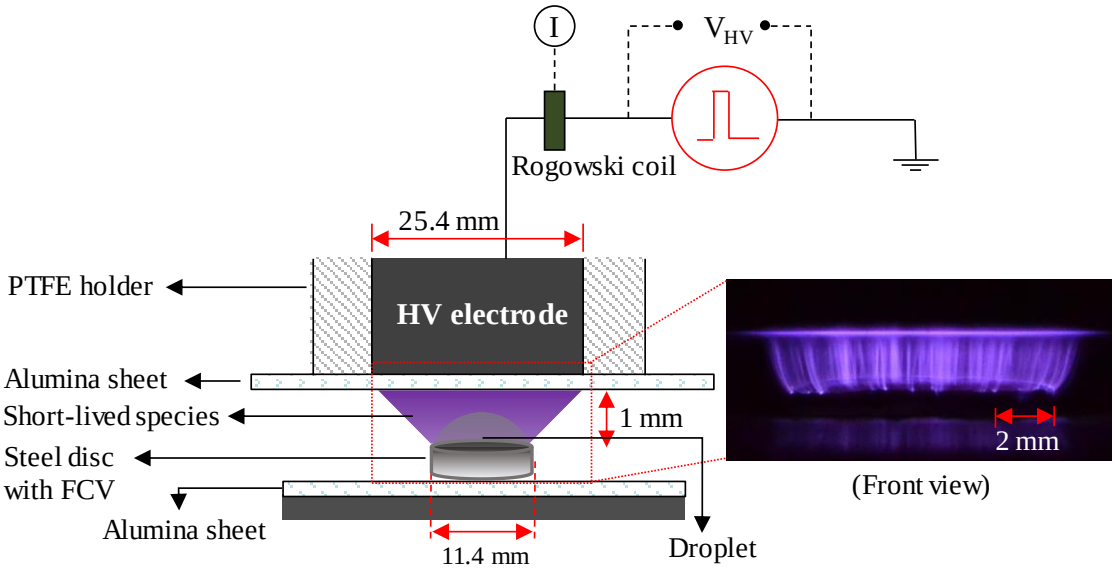

Figure 3.2. Schematic of the nanosecond-pulsed direct DBD used for the treatment of FCV samples. A photograph of the front view of the discharge is shown on the right.

The direct DBD (figure 3.2) consists of a copper rod of 25.4 mm diameter that acts as the high voltage electrode. A polytetrafluoroethylene (PTFE) tube served as a holder for this electrode. The base of the electrode was covered by an alumina sheet with a thickness of 380 µm. The steel disc on which the virus sample was applied, mounted on an aluminum ground electrode covered with another alumina sheet of the same thickness, acted as the counter electrode. A nanosecond pulse generator (NPG-18/3500N) was used to generate a discharge between the powered electrode and the surface of the steel disc placed at a distance of 1 mm. The voltage pulses were applied at a repetition frequency of 100 Hz and the amplitude was adjusted from 18.8 kV to 21.6 kV to change the energy per pulse. Applied voltage and current in the circuit were recorded using a HV probe (Tektronix

P6015A) and a Rogowski coil (Pearson 6595). The energy in the discharge was calculated as the product of voltage and current waveforms after correction of the phase shift between the probes. The samples were exposed to a continuous burst of 2000 pulses at different pulsing energies of 0.3, 0.5, 1.0, and 1.5 mJ.

(c) Surface DBD

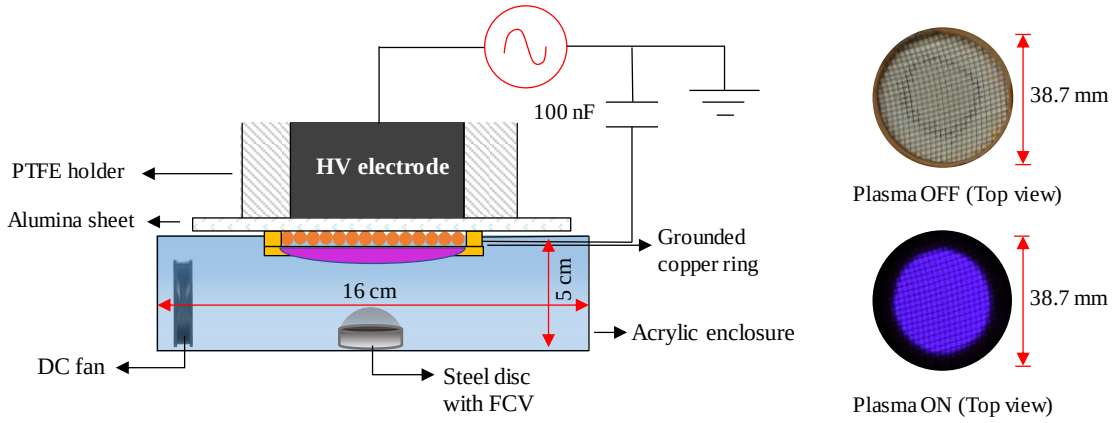

Figure 3.3. Schematic of the surface DBD batch reactor used for the treatment of FCV samples. Photographs of the electrode are shown on the right in the plasma OFF and ON conditions.

The surface DBD reactor (figure 3.3) consists of a copper rod with a diameter of 25.4 mm as the high voltage electrode and a copper ring to which a mesh is attached as the grounded electrode. The two electrodes were separated by a sheet of alumina with a thickness of 380 µm. The plasma was driven with AC sinusoidal HV signals generated by a high-voltage amplifier (Trek PD05034) at a frequency of 1 kHz and amplitude modulated at a frequency of 10 Hz with a duty cycle modulation of 20%.

This plasma source was mounted in a batch reactor with a volume of 480 cm^3, as shown in figure 3.3, for the treatment of virus samples. The bottom of the reactor on which the

samples were placed had an area of 96 cm^2. The enclosure, made of acrylic, accommodated a DC-driven fan to enhance the mixing of reactive species in the batch reactor. The discharge was ignited for a period of 1.5 and 3 minutes and then switched off. The energy deposited in the plasma per unit area of the batch reactor has been reported in table 3.1 for each of the experimental conditions used in this work. The recombination of ozone after switching off the plasma was relatively slow (see further) and the samples remained for up to 14 minutes in the box after plasma treatment. The discharge power was fixed at 0.7 W, corresponding to an optimal energy efficiency of O_3 production in the reactor.

Table 3.1.: Treatment conditions used for the surface DBD discharge at 0.70 W for the treatment of FCV samples.

Power (W)	Energy/Area (J/cm^2)	Plasma ON (min)	Plasma OFF (min)
0.70	0.66	1.5	3.5
		1.5	7
		1.5	14
	1.31	3	3.5
		3	7
		3	14

3.2.2. UV-C system

A UV-C lamp (Analytik Jena, UVP 34-0007-01), operating at a rated power of 8 W, was mounted on an adjustable stand. With an axial length of 29 cm, this cylindrical low-pressure lamp emits UV-C radiation at a central wavelength of 254 nm. The lamp was shielded by a reflective aluminum panel on the top to maximize irradiance in the region

under the lamp. To control the UV flux, a variable autotransformer was used to operate the lamp. The FCV samples were placed on a horizontal surface at a perpendicular distance of 30 cm from the lamp at the location of the maximum irradiance corresponding to 340 $\mu W \cdot cm^{-2}$. An experimental schematic is shown in figure 3.4. An autotransformer allowed the extension of the treatment times to a few minutes by reducing the electrical power of the lamp. This enabled us to more easily determine the inactivation effects of a range of UV-C fluence.

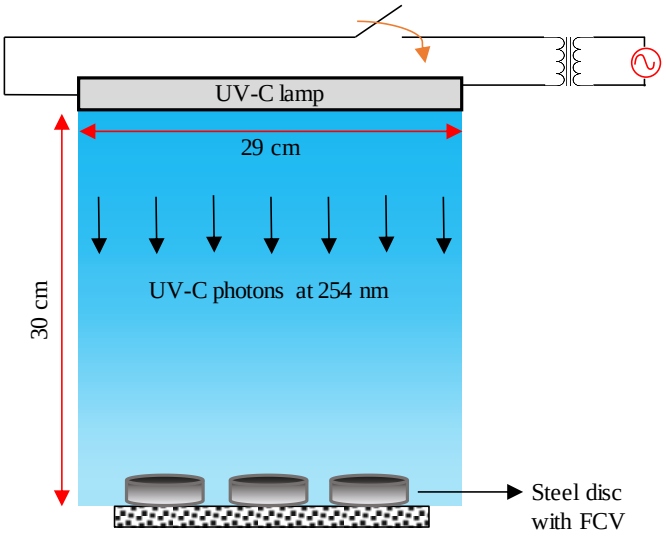

Figure 3.4. Schematic of the UV-C disinfection system used for the treatment of FCV samples.

3.2.3. Virus sample preparation and disinfection protocols

Feline calicivirus (strain 255) was propagated, concentrated, and titrated in Crandell-Reese feline kidney (CRFK) cells as described previously in [53]. Plasma treatments were performed on virus samples at least in triplicates. Averaged results are presented along with the associated standard deviation.

Aliquots (20µl) of concentrated FCV were spread aseptically on sterile stainless steel discs with a diameter of 11.4 mm. The virus samples were dried using forced air flow at room temperature in a biosafety cabinet for 30-45 minutes prior to plasma treatment. All plasma setups were operated at fixed operational conditions as mentioned above. Immediately after the plasma or UV treatment, the sample was transferred into a 10 ml sterile plastic falcon tube containing 500 µl of the elution buffer (3% beef extract + 0.05M glycine solution pH 7.2). To elute the surviving virus, all tubes were vortexed for at least one minute and then the eluates were used for virus titration. Briefly, 10-fold serial dilutions of eluates were inoculated in CRFK cell monolayers contained in 96-well microtiter plates. Three wells were used per dilution and the Karber method [30] was used for determination of virus titers.

(a) Dry and wet virus samples

The treatment of dry samples was performed by the 2D DBD and the UV lamp only. For treatment of wet samples, steel discs spiked with the virus were moistened prior to exposure to 2D DBD, nanosecond pulsed direct DBD, and UV-C lamp. In case of treatment using 2D DBD and UV-C lamp, the sample surface was moistened by spraying distilled water of 20±5µl. The surface was sprayed with water prior to the start of treatments and consecutively after every two minutes in case of the 2D DBD to ensure that a liquid layer is maintained. For the ns pulsed DBD, a droplet of 30µl of distilled water was pipetted onto the dried virus sample on the steel disc prior to exposure.

(b) Direct and indirect exposure of virus samples

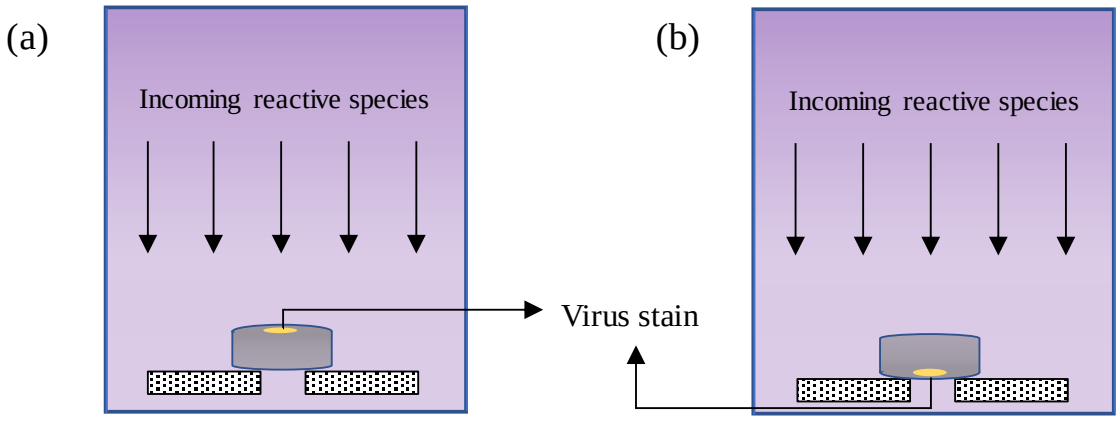

Figure 3.5. Schematics illustrating (a) direct exposure, and (b) indirect exposure of virus stains on stainless steel discs to reactive species generated in a disinfection system.

In a plasma flow-through or UV treatment system, the orientation of the sample determines if it is being exposed to the reactive species directly or indirectly. Experiments involving direct exposure were performed by placing the virus-spiked surface of the steel disc such that it faces the discharge effluent or the UV radiation, as shown in figure 3.5(a). Figure 3.5(b) shows the configuration for indirect exposure which was performed with the 2D DBD and UV-C only. During indirect exposure, the steel disc was flipped so the virus-spiked surface faced away from the discharge effluent or UV radiation. Four small plastic spacers were used to elevate the disc from the surface of the teflon block used to hold the samples to enable diffusion of species towards the location of the virus stain and thus facilitate volumetric treatment of the substrate.

3.2.4. Gas-phase O_3 and NO_2 densities measurements

Exposure of the virus samples during remote plasma treatment leads to inactivation due to the action of long-lived reactive species. Air plasmas generate an abundance of reactive oxygen and nitrogen species that are known for their antimicrobial attributes [1], [15]. To characterize the remote treatment conditions, the densities of selected reactive oxygen and nitrogen species (O_3 and NO_2) were measured at the location of the virus sample. UV absorption spectroscopy was used to measure the ozone densities in the discharge effluent using a low pressure Hg/Ar lamp and a broadband spectrometer (Avantes AvaSpec-2048). This measurement was performed as described in detail in [19]. A commercially available gas analyzer (Enerac 500, ENERAC) was used to monitor the gas-phase NO_2 concentration in the discharge effluent. The sampling of the gas was also performed at the location of the virus sample.

3.2.5. UV-C fluence

The UV-C irradiance was measured by a UV light meter (UVC Light Meter 850010, Sper Scientific Environmental Measurement Instruments, Scottsdale, AZ, USA). The UV lamp, operating at a rated power of 8 W, was a line source of light emission whose radiative flux distribution was studied using the UV meter. The irradiance, I(x,y), was measured on a horizontal plane at a distance z from the lamp at each of the nodes of the 4×4 cm grid, across the field of illumination. These measurements were performed with the lamp placed at a perpendicular distance (z) of 5 cm, 10 cm, and 20 cm from the horizontal plane. The irradiance was numerically integrated using trapezoidal rule across the entire area to

evaluate the total radiant power. The difference in total radiant power remains within 3% as the treatment distance is varied between 5 and 20 cm. The electrical efficiency (η) is calculated as the ratio of the radiant power to the electrical power drawn by the lamp.

$$\eta = \frac{\int I(x,y)\, dA}{\text{Electrical power}} \times 100$$

For practical reasons, only the area with an irradiance greater than half of the maximum was considered for determining the energy cost of the system.

To determine the possible role of plasma-generated UV radiation in plasma-based decontamination, the UV-C irradiance was measured at a distance of 1 cm from the plasma for remote plasma treatment sources, providing an upper limit of the UV irradiance at the position of the virus sample.

3.2.6. Statistical analysis and kinetics of inactivation

All the virus inactivation experiments were performed in triplicates. The one-way analysis of variance (one-way ANOVA) performed by the F-test was carried out to evaluate the statistical significance of differences between the treated and control samples. Fisher's least significant difference (Fisher's LSD) test was used for comparisons between means. STATISTICA software v. 10 (Statsoft Inc., Tulsa, OK, USA) was used for statistical analysis. The D-value in case of plasma-based and UV-based inactivation was defined as the time in minutes and UV-C dose in mJ/cm^2 needed to achieve 1 $\log_{10}$ reduction, respectively. Regression analysis was performed on the first 3 or 4 data points (virus inactivation >1 $\log_{10}$) to obtain the D-value. The D-value can be expressed as:

$$\log_{10}(N_t) = \log_{10}(N_0) - \frac{t}{D} \quad \text{(Eq. 1)}$$

where N_t is the titer of surviving FCV after treatment, N_0 is the initial FCV titer and t is the treatment time in minutes. The FCV titer is expressed as $\log_{10}$ $TCID_{50}$/100µl of eluent. For plasma treatments, D is expressed in the units of minutes. For UV-C treatment, t is replaced by the fluence, yielding a D-value with units of $mJ \cdot cm^{-2}$.

3.3. Results and Discussion

3.3.1. Reactive species

The time evolution of reactive species generated by a microdischarge in ambient air has been modeled by Eliasson and Kogelschatz [83]. Based on this study, the dominant virucidal species in the effluent of DBDs with a gas residence time of 786 ms, as is the case in our work, are O_3, NO_2, and possibly N_2O_5. In addition, short-lived radicals like OH and O, and ions can contribute to the observed virucidal effects when the discharge is in direct contact with the substrate. The measured concentrations of O_3 and NO_2 at the location at the virus sample for the 2D DBD setup are 140 and 83 ppm, respectively.

Shimizu *et al.* [26] studied a surface discharge operating in ambient air and proposed the existence of different regimes of operation based on power density during which either O_3 or NO_x are the dominant species. The transition power density was found to be 0.1 $W \cdot cm^{-2}$. The surface DBD used in this work was operated at a low power density of 0.06 W/cm^2 and primarily generates O_3. Hence, we only report O_3 concentrations for this setup in table 3.2.

Table 3.2. Concentrations of reactive species measured in the indirect plasma treatment setups for the inactivation of FCV coated steel discs.

Plasma power (W)	Treatment time (min)		[O_3]	
	Plasma ON	Plasma OFF	C (ppm)	Ct ($mg \cdot min \cdot l^{-1}$)
0.70	1.5	3.5	130	1.15
	1.5	7	120	1.99
	1.5	14	108	3.54
	3	3.5	267	2.74
	3	7	231	4.44
	3	14	186	7.24

The inactivation effect of O_3 is widely characterized as a function of the Ct value, which is the product of the concentration of O_3 and the interaction time between the sample and the gas. The O_3 Ct value in the 2D DBD setup is 0.82 $mg \cdot min \cdot l^{-1}$. The concentration of O_3 in the surface DBD setup is a time-dependent function, and the corresponding Ct value is calculated as:

$$\mathrm{Ct} = \int \mathrm{C(t)}\ \mathrm{dt}$$

The Ct values ($mg \cdot min \cdot l^{-1}$) corresponding to the experimental conditions used for the treatment of FCV samples have been reported in table 3.2. The temporal evolution of [O_3] in the surface DBD batch reactor is shown in figure 3.6 for two different plasma ON times (1.5 and 3 minutes).

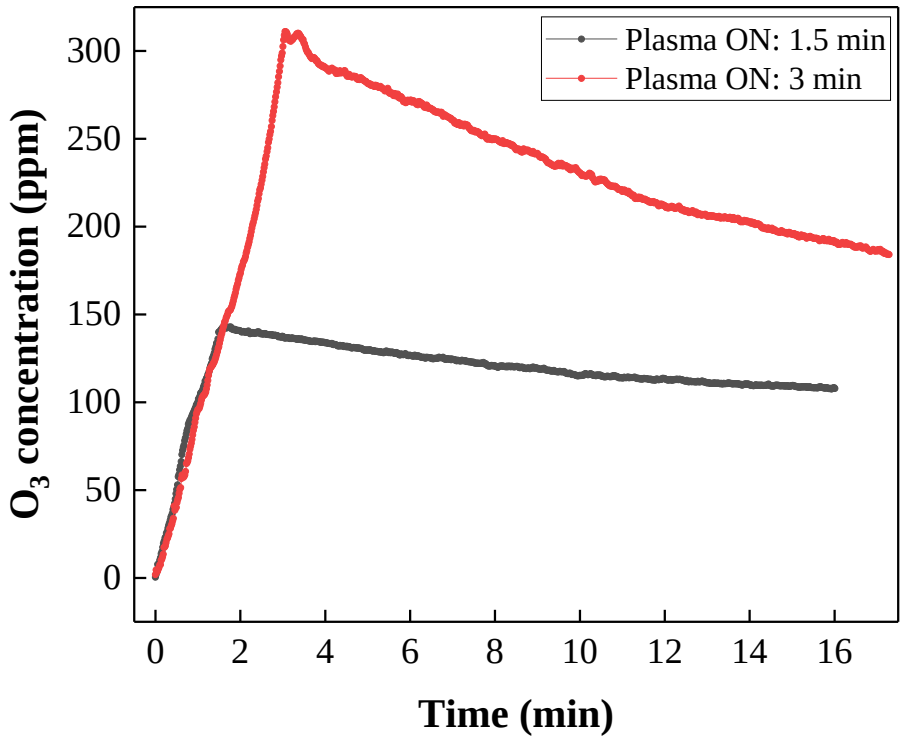

Figure 3.6. Gas-phase O_3 concentration measured in the surface DBD batch reactor at a discharge power of 0.70 W as a function of time. The plasma ON time is 1.5 and 3 minutes.

3.3.2. UV radiation

The UV-C flux remains below 0.4 mJ·cm^{-2} across all the experimental conditions for the plasma treatments. This is two orders of magnitude lower than the UV-C flux required for the inactivation of FCV samples [36].

The spatial distribution of irradiance from the UV-lamp on a horizontal plane at a distance of 10 cm is shown in figure 3.7. The degree of inhomogeneity and the magnitude of maximum fluence is highest when the lamp is placed closest to the horizontal plane. This exposes the practical limitations encountered during the use of ultraviolet light from a line

source of light emission. As a consideration of this implication, it is important to note that the use of UV-C light as a disinfection system involves irregular irradiation and necessitates excessive treatment to ensure complete inactivation of the pathogen. To calculate the electrical efficiency of the UV-C lamp, the irradiance of the lamp only in the region where the irradiance is equal to or larger than half the max irradiance was considered. The average electrical efficiency of the UV lamp has been estimated to be 10.7% with a standard deviation of 1.6% resulting from measurements at three different treatment distances (5, 10, and 20 cm). This value of energy efficiency has been considered in estimating the electrical energy costs of using UV-C disinfection systems.

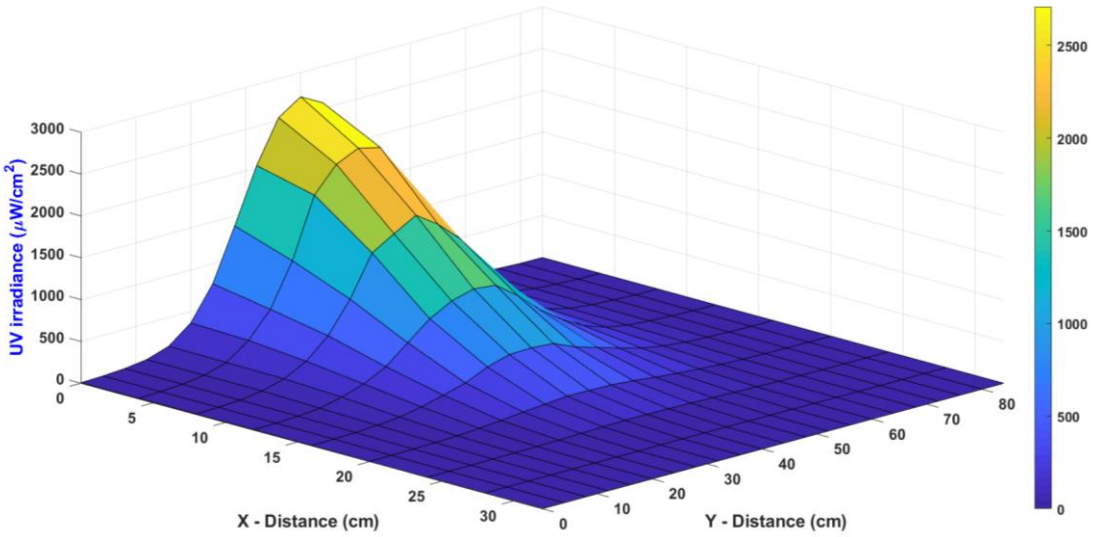

Figure 3.7. Spatial distribution of UV-C irradiance from the UV-C lamp on a horizontal plane at a perpendicular distance of 10 cm. The lamp is placed along the Y-axis at X = 0. The irradiance is only shown for one side of the lamp as it is symmetric with respect to the longitudinal axis of the lamp.

3.3.3. Virus inactivation by CAP and UV-C under direct exposure

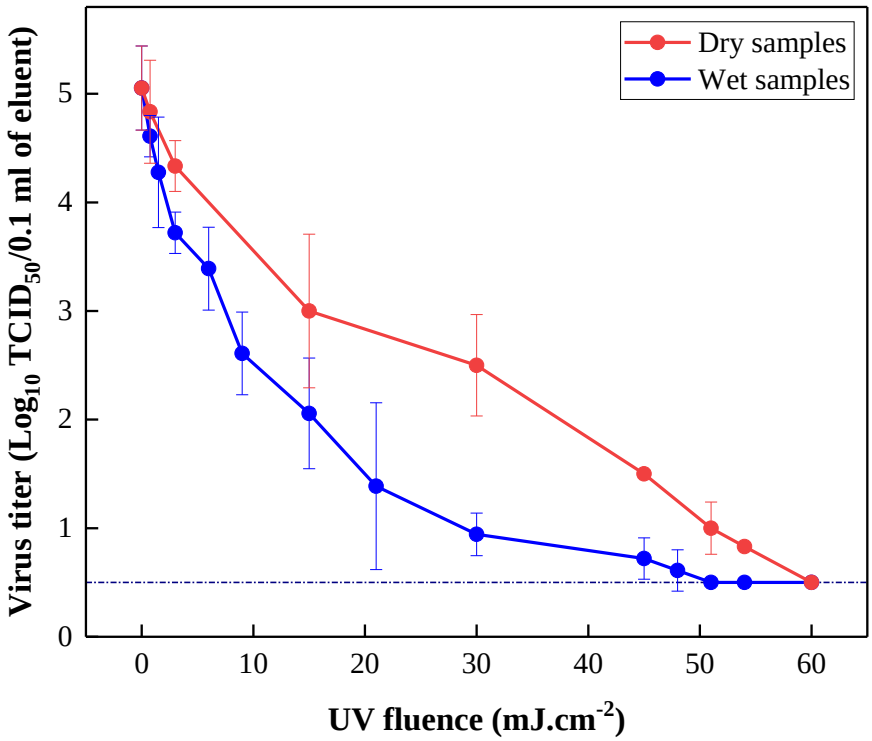

Figure 3.8. Inactivation of FCV coated on stainless steel discs exposed to UV-C radiation as a function of its fluence. The samples were treated in both dry and wet surface conditions. The detection limit of the method is indicated with a dashed line.

As shown in figure 3.8, UV-C exhibits a fluence-dependent reduction in FCV titer for both dry and wet virus samples. Complete inactivation (>5.0 $\log_{10}$) occurred at a UV-C fluence of 51 mJ·cm^{-2} and 60 mJ·cm^{-2} for wet and dry samples, respectively. As shown by the kinetic analysis of viral inactivation (table 3.3), the rate of inactivation of wet samples by UV-C was significantly higher than that of dry samples.

Table 3.3. D-values of FCV inactivation using plasma-based and UV disinfection systems. Statistical analysis was performed using log-linear regression model.

Treatment	Sample type	FCV initial titer (Log_{10} TCID50/100µl eluent)	D-Value	R^2
2D DBD	Wet	5.39	0.22 ± 0.03 min	0.94
	Dry	5.39	1.21 ± 0.32 min	0.88
UV-C	Wet	5.05	2.29 ± 0.18 mJ/cm^2	0.94
	Dry	5.05	7.68 ± 0.82 mJ/cm^2	0.98

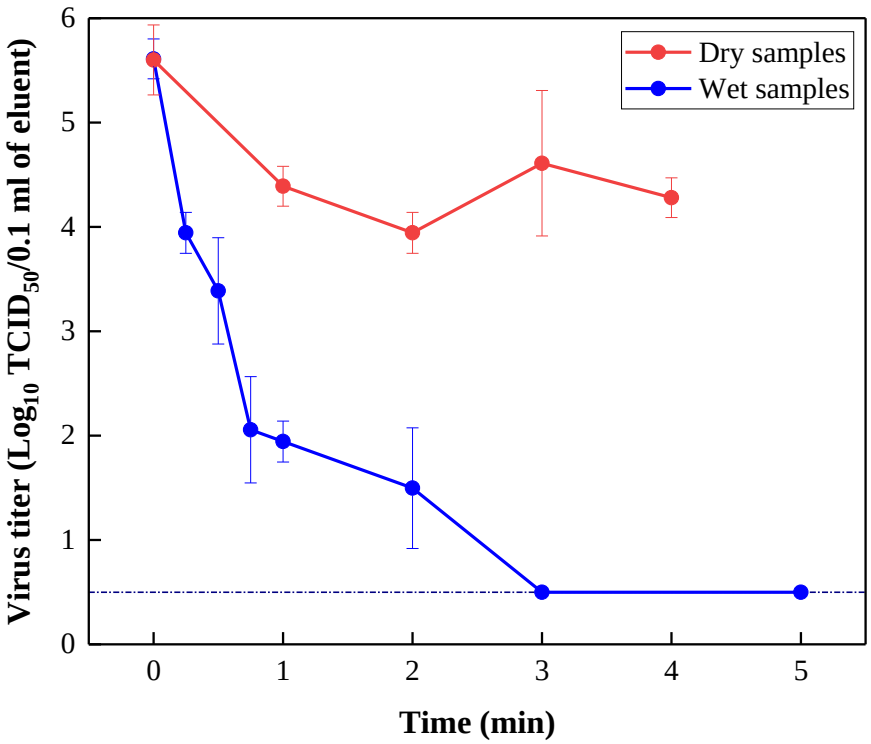

Figure 3.9. Gas-phase inactivation of FCV coated stainless steel discs using the 2D DBD air plasma as a function of treatment time. The samples were exposed to the discharge effluent in both dry and wet surface conditions. The detection limit of the method is indicated with a dashed line. (Data is taken from [21])

Similarly, the treatment of wet samples of FCV by the 2D DBD showed significant time-dependent reductions in FCV titer (figure 3.9) with complete inactivation at 3 min. Exposure of dry samples to the 2D DBD showed limited reductions in FCV titer with a significantly larger D-value (see table 3.3). Figure 3.10 shows the effect of pulsed direct DBD at increasing energy per pulse on wet FCV samples. Complete inactivation of FCV was obtained after exposure to a burst of 2000 pulses at an energy per pulse of 1 mJ.

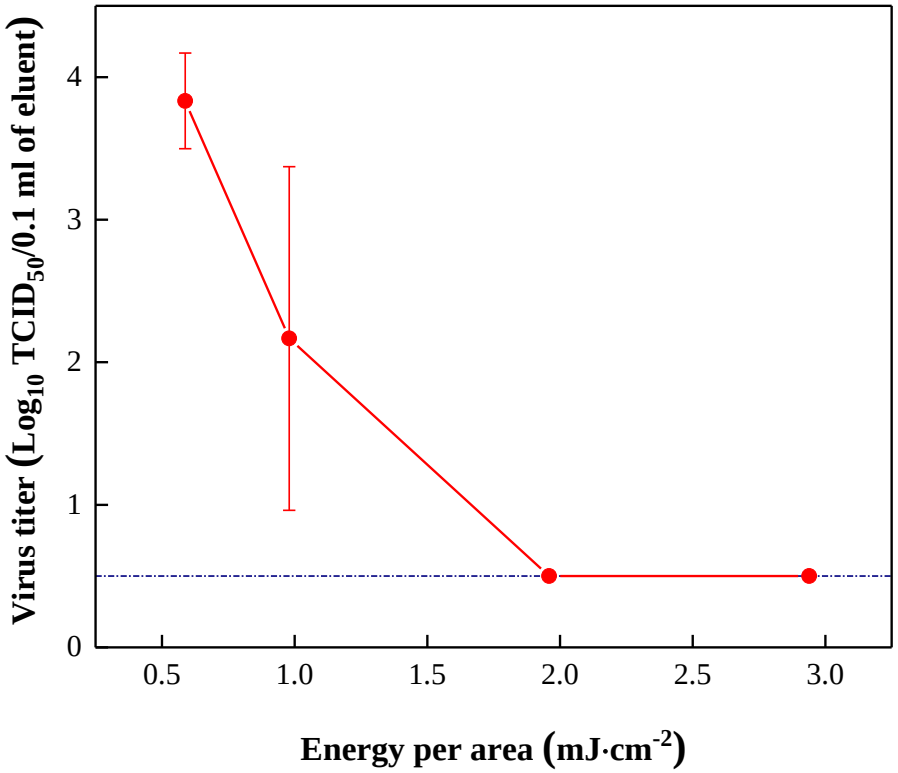

Figure 3.10. Inactivation of FCV coated on stainless steel discs exposed to the nanosecond pulsed direct DBD operating at different discharge powers. The samples were treated in wet surface conditions only with a burst of 2000 pulses. The detection limit of the method is indicated with a dashed line.

The results show that UV-C is able to inactivate FCV on both wet and dry surface while remote plasma treatment is highly effective for wet FCV samples. The efficacy of remote plasma treatment on dry virus samples in limited.

3.3.4. Comparison of direct and indirect exposure to cold plasma and UV-C

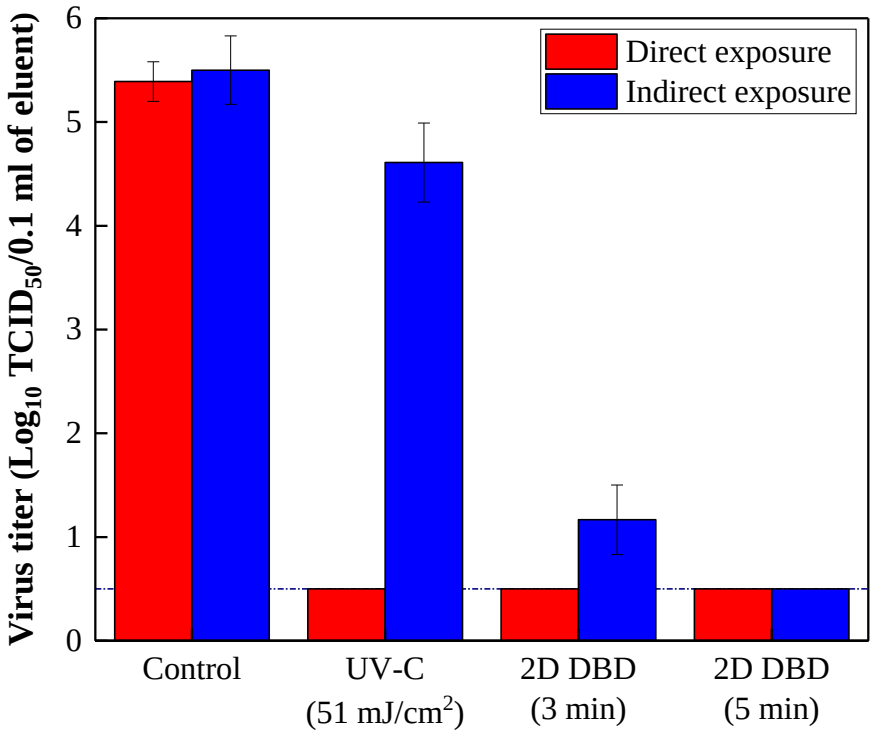

Figure 3.11. Inactivation of FCV coated on stainless steel discs treated with 2D DBD air plasma and UV-C radiation. Differences in effects based on the orientation of the spiked surface with respect to the reactive species generated by plasma source or UV lamp are illustrated. The detection limit of the method is indicated with a dashed line.

Figure 3.11 shows a comparison of virus inactivation observed in the case of direct and indirect exposure of samples to UV-C radiation and remote plasma. Compared to complete inactivation during direct exposure, indirect exposure to UV-C radiation led to <1 $\log_{10}$ inactivation of FCV. This is consistent with the known directionality of UV treatment. On

the contrary, direct and indirect exposure to the plasma effluent of the 2D DBD showed significant reductions in the virus titer. At 3 minutes, 5 and 4.33 $\log_{10}$ of FCV were inactivated by direct and indirect exposure, respectively. Complete inactivation of FCV was achieved by direct and indirect exposure for 5 min. These results indicate that remote plasma treatment enables a non-directional volumetric treatment of irregular 3D objects such as fruits and fresh produce. This observation demonstrates a significant advantage of remote plasma treatment over UV radiation in that the reactive species generated by cold plasmas, unlike UV radiation, are not limited by significant shadowing effects [80], [82].

3.3.5. Plasma treatment in a batch reactor

The results of remote plasma treatment reported in previous sections were obtained by experiments performed in a flow-through reactor. This approach does not enable effective utilization of the plasma-generated reactive species as it only allows a one-time interaction between reactive species and the virus samples before the species are blown away through the exhaust. To enhance the effective use of the plasma-generated reactive species, we have also evaluated the inactivation of FCV samples in a batch reactor (see figure 3.3).

Figure 3.12 shows the inactivation of FCV samples caused by the surface DBD operating at a constant discharge power of 0.70 W in a batch reactor. The plasma ON time was fixed at 1.5 and 3 minutes corresponding to an energy consumption of 63 J and 126 J, respectively. The corresponding O_3 concentrations in the batch reactor at the end of plasma treatment were ~140 and 310 ppm, respectively. The plasma OFF time was varied from 3.5 to 14 minutes to allow longer interaction between the reactive species and the sample

without increasing the energy deposition. The Ct values for each treatment condition are reported in table 3.2. Figure 3.12 shows that complete inactivation was achieved with the lower energy condition for a plasma OFF time of 14 minutes. This corresponds to a Ct value of 3.54 $mg \cdot min \cdot l^{-1}$ and is consistent with virus inactivation observed in [21] when FCV samples were exposed to ozone at a fixed concentration produced by an Ar+20% O_2 DBD during the treatment.

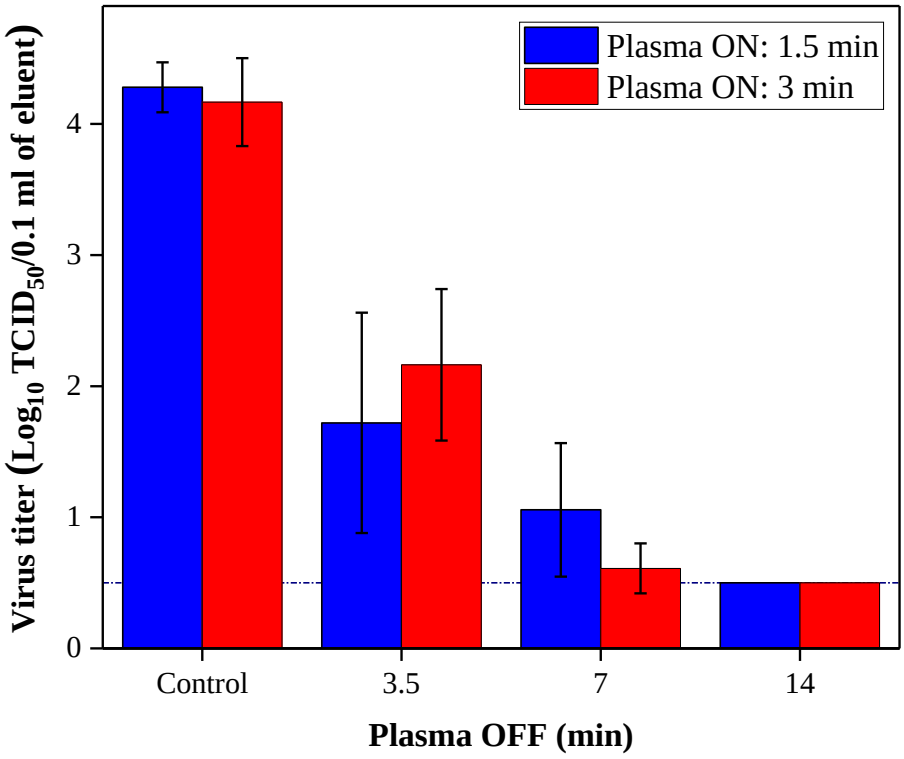

Figure 3.12. Inactivation of FCV samples observed as a function of plasma OFF time when the surface DBD was operated in an enclosed volume. The plasma was switched ON for 1.5 and 3 minutes at a discharge power of 0.7 W. The detection limit of the method is indicated with a dashed line.

3.3.6. Energy consumption

To determine the operational costs of plasma as a disinfection technology, we seek to provide estimates of energy consumption corresponding to complete inactivation of FCV using cold plasmas and UV-C per unit area. Table 3.4 shows a comparison of all the decontamination sources used in terms of electrical power and energy consumed per unit volume of gas treated for complete inactivation (~5 $\log_{10}$ $TCID_{50}$). With the nanosecond pulsed direct discharge, complete inactivation was achieved with a burst of 2000 pulses at 1 mJ corresponding to an energy consumption of 2 J. This corresponds to an energy per area of 1.96 $J \cdot cm^{-2}$, which remains about five times higher than the energy unit area for decontamination by the UV-C lamp.

The surface DBD, operating in a batch reactor with a volume of 480 cm^3, utilized O_3 as the dominant reactive species to achieve complete inactivation at an energy consumption of 63 J. This corresponds to an energy requirement of 0.66 $J \cdot cm^{-2}$, assuming that the lower surface area of the reactor is effectively treated. This value is similar to the energy requirement per unit area for inactivation of FCV using UV-C. Commercial ozone generators utilizing either DBDs or corona discharges are known to produce ozone generation with efficiencies of 150 g O_3/kWh with air as the feed gas [84]–[86], while the surface DBD has an O_3 generation efficiency of 8 g/kWh. This suggests that it might be possible to improve the energy efficiency of the reactor.

Table 3.4. Comparison of the energy requirements for complete inactivation (>4 log10) of FCV coated stainless steel discs by different plasma sources and UV-C. A dash implies that the quantity has not been measured or is not applicable for this condition.

Disinfection system	UV-C Irradiance ($\mu W/cm^2$)	Power (or) Energy	E/V (J/L)	E/A (J/cm^2)
UV-C lamp	340	8 W	-	0.48
Direct DBD	?	1 mJ/pulse	-	1.96
Surface DBD	< 1	0.7 W	131.2	0.66
2D DBD*	< 1	14.5 W	53	0.13-0.53

*Estimates based on simple reactor model

The concept of a batch reactor could be extended to the 2D DBD as well. During indirect plasma treatment using the 2D DBD, the plasma treats the gas rather than the sample directly. A treatment time of 3 minutes leads to the treatment of ~50 liters of air in a flow-through reactor operating at 16.4 SLM. This corresponds to an energy consumption of 53 J/L. As the flow-through reactor used with the 2D DBD is not effective in using the generated reactive oxygen and nitrogen species, let us suppose that the treatments could be performed in a batch reactor with a capacity of 1 liter ($20\times20\times2.5$ cm^3 or $10\times10\times10$ cm^3). With an assumption that the reactive species responsible for the virucidal effects have lifetimes in excess of 3 minutes, an effective treatment of the lower surface area (400 cm^2 or 100 cm^2) can be performed by treating only one liter of air and leaving it in the batch reactor for 3 minutes. This corresponds to an energy consumption per unit area of 0.13-0.53 $J\cdot cm^{-2}$. The long lifetime of the reactive species (3 minutes) is a realistic expectation

in view of the slow decay of the reactive species responsible for decontamination (see also, figure 3.6). The flow-through reactor measurements with the 2D DBD air plasma can achieve complete inactivation of FCV samples at a Ct value of 0.8 $mg \cdot min \cdot l^{-1}$, while a Ct value of 3.5 $mg \cdot min \cdot l^{-1}$ is required for complete inactivation with the surface DBD. Given the greater effectiveness in FCV inactivation of the reactive species generated by the 2D DBD in comparison to the ozone-based surface DBD, it should be possible to further optimize remote plasma treatment systems. This suggests that remote plasma treatment in an appropriately designed batch reactor could be operating with similar or even better energy efficiencies than conventional UV disinfection technology.

3.4. Conclusion

A comparative study of FCV inactivation by different plasma sources and UV-C was performed in terms of virucidal efficacy and energy efficiency. Our results indicate that UV-C and all studied plasma sources can completely decontaminate FCV coated steel discs with a wet surface. While UV-C radiation and direct plasma treatment are able to effectively inactivate dry virus samples, remote plasma treatment is only effective on wet virus samples. Direct contact plasma treatment is four times more energy-intensive compared to UV-C treatment but improved energy efficiency might be attainable by further optimization of the plasma source and its operating conditions. We showed that the plasma-generated species are not limited by shadowing effects, a key advantage of remote plasma treatment compared to UV-C. Effective utilization of the plasma-generated reactive species in a batch reactor enables lower energy costs of decontamination using a surface discharge

to a level that is comparable to that of UV-C based decontamination. Theoretical estimates based on a model reactor design using a volumetric air plasma suggest the potential for further reduction in the energy costs of plasma-based decontamination. While further detailed studies on different pathogens and impact on food samples are required, the results within this work shows that the potential of cold plasma as a non-thermal technology for food industry applications should not be limited by operational costs.

Conclusion

In this work, we developed different atmospheric pressure plasma sources to study their capabilities for surface decontamination of stainless steel discs. Experiments to study the antimicrobial activity were performed on feline calicivirus (FCV), a surrogate of human Norovirus, and *Salmonella Heidelberg*. Both pathogens are leading causes of food borne illnesses. One of the plasma sources, the 2D DBD, was characterized extensively and its dominant chemical pathway towards decontamination was identified. The influence of surface humidity on the effectiveness of plasma-based decontamination was studied through quantification of reactive species in the aqueous phase. The energy efficiency of different plasma sources was reported and compared with that of UV-C to provide an idea of the operational costs of the technology.

For a comparison of the effectiveness of surface decontamination by plasma treatment, DBDs and gliding arc discharges were operated with air as the feed gas at atmospheric pressure. Plasma sources enabling direct and remote treatment of the substrates were also compared. Across all the sources, FCV was seen to be more susceptible to the plasma-generated reactive species than Salmonella. While direct treatment was effective against both dry and wet samples, remote plasma sources exhibited negligible decontamination against dry samples. The efficacy of remote plasma treatment was significantly enhanced by the presence of humidity on the surface of the substrate and complete inactivation of wet samples was achieved by all the plasma sources. The requirement for higher energy deposition into the gliding arc to achieve decontamination comparable to the remote DBDs

is attributed to the much lower Henry's law constant of NO, which is the dominant species generated by the gliding arc, compared to the Henry's law constant of NO_2, one of the dominant species generated by the DBDs. Synergistic effects due to the interaction between O_3 and NO_2 in the afterglow of the DBDs was verified through positive control tests, and a kinetic model suggests a strong correlation between the gas-phase concentration of N_2O_5 and the observed virucidal effects. The flexibility offered by remote plasma treatments is indispensable in making the adoption of plasma technology into the food industry possible, particularly in view of the freedom it allows in food substrate morphology.

A detailed knowledge on the influence of surface humidity on the effectiveness of plasma treatment is imperative to determine the working conditions for optimal plasma treatment. This optimum treatment is typically impacted by transport of reactive species from the gaseous effluent to the liquid that covers the microorganism on the substrate. Decontamination using plasma treatment and positive control tests using O_3 and NO_2 suggest that the inactivation was most effective when the thickness of the water layer covering the substrate was minimum. This effect was consistent with an increase in reactive nitrogen species concentrations with decreasing volume of the liquid layer.

Although several existing studies report good antimicrobial activity using a variety of plasma sources, none of the studies focuses on the costs of operation of the plasma technologies. A comparison was drawn among different plasma sources and UV-C based on their virucidal efficacies and energy efficiencies. Direct plasma treatment was found to be four times more energy-intensive than UV-C technology. A batch reactor protype used

with a surface discharge predominantly generating O_3 enabled effective utilization of the reactive species and lowered the energy costs of plasma-based decontamination to a level that is comparable to that of UV-C based decontamination. While UV-C radiation can effectively inactivate substrates with a dry surface, the directional nature of UV-photons is a major disadvantage of this conventional technology.

All the experiments performed in this work study surface decontamination of metal discs spiked with a species of virus or bacteria. As an effort towards confirming the extent of applicability of our results, plasma treatments are to be performed on more pathogens classified based on their pathological or biological characteristics. As a further step, it is required to extend the application of plasmas to food substrates and assess possible off-target effects on food. This will give us insights on the effects of the surface of the substrate and help us determine plasma conditions required to meet the standards of the industry. From a practical standpoint, it would be advantageous to develop plasma sources that are scalable and can operate in air to minimize costs and chemical waste streams.

The results within this work demonstrate the capability cold plasmas hold towards being a sustainable and green non-thermal decontamination technology.

Bibliography

[1] D. B. Graves, "The emerging role of reactive oxygen and nitrogen species in redox biology and some implications for plasma applications to medicine and biology," *J. Phys. D. Appl. Phys.*, vol. 45, no. 26, 2012.

[2] C. A. J. Van Gils, S. Hofmann, B. K. H. L. Boekema, R. Brandenburg, and P. J. Bruggeman, "Mechanisms of bacterial inactivation in the liquid phase induced by a remote RF cold atmospheric pressure plasma jet," *J. Phys. D. Appl. Phys.*, vol. 46, no. 17, 2013.

[3] P. Lukes, E. Dolezalova, I. Sisrova, and M. Clupek, "Aqueous-phase chemistry and bactericidal effects from an air discharge plasma in contact with water: Evidence for the formation of peroxynitrite through a pseudo-second-order post-discharge reaction of H2O 2 and HNO2," *Plasma Sources Sci. Technol.*, vol. 23, no. 1, p. 015019, 2014.

[4] J. Foster, B. S. Sommers, S. N. Gucker, I. M. Blankson, and G. Adamovsky, "Perspectives on the interaction of plasmas with liquid water for water purification," *IEEE Trans. Plasma Sci.*, vol. 40, no. 5, pp. 1311–1323, 2012.

[5] D. Radin, "Transmission due to contaminated fresh fruit and vegetables dragoslava radin," vol. 64, no. 4, pp. 1405–1411, 2012.

[6] "Centers for Disease Control and Prevention: Norovirus," 2016. [Online]. Available: http://www.cdc.gov/norovirus/.

[7] C. N. Berger *et al.*, "Fresh fruit and vegetables as vehicles for the transmission of human pathogens," *Envrionmental Microbiol.*, vol. 12, no. 9, pp. 2385–2397, 2010.

[8] S. Zhao *et al.*, "Antimicrobial resistance in Salmonella enterica serovar Heidelberg isolates from retail meats, including poultry, from 2002 to 2006," *Appl. Environ. Microbiol.*, vol. 74, no. 21, pp. 6656–6662, 2008.

[9] N. Misra, B. Tiwari, K. Raghavarao, and P. Cullen, "Nonthermal Plasma Inactivation of Food-Borne Pathogens," *Food Eng. Rev.*, vol. 3, no. 3–4, pp. 159–170, 2011.

[10] G. Fridman *et al.*, "Comparison of Direct and Indirect Effects of Plasma on Bacteria," *Plasma Process. Polym.*, vol. 4, no. 4, pp. 370–375, 2007.

[11] B. G. Dasan, B. Onal-Ulusoy, J. Pawlat, J. Diatczyk, Y. Sen, and M. Mutlu, "A New and Simple Approach for Decontamination of Food Contact Surfaces with Gliding Arc Discharge Atmospheric Non-Thermal Plasma," *Food Bioprocess*

Technol., vol. 10, no. 4, pp. 650–661, 2017.

[12] T. T. Gupta, J. S. Matson, and H. Ayan, "Antimicrobial Effectiveness of Regular Dielectric-Barrier Discharge (DBD) and Jet DBD on the Viability of Pseudomonas aeruginosa," *IEEE Trans. Plasma Sci.*, vol. 2, no. 1, pp. 68–76, 2017.

[13] D. Dobrynin, G. Fridman, G. Friedman, and A. Fridman, "Physical and biological mechanisms of direct plasma interaction with living tissue," *New J. Phys.*, vol. 11, p. 115020, 2009.

[14] X. Lu *et al.*, "The roles of the various plasma agents in the inactivation of bacteria," *J. Appl. Phys.*, vol. 104, no. 5, p. 053309, 2008.

[15] M. Laroussi and F. Leipold, "Evaluation of the roles of reactive species, heat, and UV radiation in the inactivation of bacterial cells by air plasmas at atmospheric pressure," *Int. J. Mass Spectrom.*, vol. 233, no. 1–3, pp. 81–86, 2004.

[16] H. A. Aboubakr *et al.*, "Virucidal effect of cold atmospheric gaseous plasma on feline calicivirus, a surrogate for human norovirus," *Appl. Environ. Microbiol.*, vol. 81, no. 11, pp. 3612–3622, 2015.

[17] S. Bekeschus, A. Schmidt, K. Weltmann, and T. Woedtke, "The plasma jet kINPen – A powerful tool for wound healing," *Clin. Plasma Med.*, vol. 4, no. 1, pp. 19–28, 2016.

[18] M. Laroussi and X. Lu, "Room-temperature atmospheric pressure plasma plume for biomedical applications," *Appl. Phys. Lett.*, vol. 87, p. 113902, 2005.

[19] G. Nayak, Y. Du, R. Brandenburg, and P. J. Bruggeman, "Effect of air flow on the micro-discharge dynamics in an array of integrated coaxial microhollow dielectric barrier discharges," *Plasma Sources Sci. Technol.*, vol. 26, no. 3, pp. 1–13, 2017.

[20] G. Nayak, J. S. Sousa, and P. J. Bruggeman, "Singlet delta oxygen production in a 2D micro-discharge array in air: Effect of gas residence time and discharge power," *J. Phys. D. Appl. Phys.*, vol. 50, no. 10, 2017.

[21] G. Nayak, H. A. Aboubakr, S. M. Goyal, and P. J. Bruggeman, "Reactive species responsible for the inactivation of feline calicivirus by a two-dimensional array of integrated coaxial microhollow dielectric barrier discharges in air," *Plasma Process. Polym.*, vol. 15, no. 1, pp. 1–12, 2018.

[22] G. El-Aragi, "Inactivation of Hepatitis C Virus Cells Using Gliding Arc Discharge," *Plasma Med.*, vol. 5, no. 1, pp. 49–55, 2015.

[23] S. Kim, Y. Cho, H. In, H. Dong, D. Cho, and A. Fridman, "Use of plasma gliding arc discharges on the inactivation of E. Coli in water," *Sep. Purif. Technol.*, vol.

120, pp. 423–428, 2013.

[24] R. Burlica, R. G. Grim, K. Y. Shih, D. Balkwill, and B. R. Locke, “Bacteria inactivation using low power pulsed gliding arc discharges with water spray,” *Plasma Process. Polym.*, vol. 7, no. 8, pp. 640–649, 2010.

[25] M. J. Pavlovich, D. S. Clark, and D. B. Graves, “Quantification of air plasma chemistry for surface disinfection,” *Plasma Sources Sci. Technol.*, vol. 23, no. 6, p. 065036, 2014.

[26] T. Shimizu, Y. Sakiyama, D. B. Graves, J. L. Zimmermann, and G. E. Morfill, “The dynamics of ozone generation and mode transition in air surface micro-discharge plasma at atmospheric pressure,” *New J. Phys.*, vol. 14, p. 103028, 2012.

[27] M. J. Pavlovich, H. W. Chang, Y. Sakiyama, D. S. Clark, and D. B. Graves, “Ozone correlates with antibacterial effects from indirect air dielectric barrier discharge treatment of water,” *J. Phys. D. Appl. Phys.*, vol. 46, no. 14, 2013.

[28] R. Brandenburg, “The bactericidal effect of surface micro-discharge plasma under different ambient conditions,” *New J. Phys.*, vol. 13, p. 023026, 2011.

[29] J. R. Topping *et al.*, “Temperature inactivation of Feline calicivirus vaccine strain FCV F-9 in comparison with human noroviruses using an RNA exposure assay and reverse transcribed quantitative real-time polymerase chain reaction-A novel method for predicting virus infectivity,” *J. Virol. Methods*, vol. 156, no. 1–2, pp. 89–95, 2009.

[30] G. Karber, “Beitrag zur kollektiven behandlung pharmakologischer reihenversuche,” *Exp Pathol Pharmocol*, vol. 162, no. 4, pp. 480–483, 1931.

[31] K. V. Nisar, M., Kassem, I. I., Rajashekara, G., Goyal, S. M., Lauer, D., Voss, S., Nagaraja, “Genotypic relatedness and antimicrobial resistance of Salmonella Heidelberg isolated from chickens and turkeys in the midwestern United States,” *J. Vet. Diagnostic Investig.*, vol. 29, no. 3, pp. 370–375, 2017.

[32] A. Hearn, “The absorption of ozone in the ultraviolet and visible region of the spectrum,” *Proc. Phys. Soc.*, vol. 78, pp. 932–940, 1961.

[33] R. A. Graham and H. S. Johnston, “The photochemistry of NO3 and the kinetics of the N2O5-O3 system,” *J. Phys. Chem.*, vol. 82, no. 3, pp. 254–268, 1978.

[34] B. Eliasson and U. Kogelschatz, “Modeling and applications of silent discharge plasmas,” *IEEE Trans. Plasma Sci.*, vol. 19, no. 2, pp. 309–323, 1991.

[35] H. Ng, H. G. Bayne, and J. a Garibaldi, “Heat resistance of *Salmonella*: the uniqueness of *Salmonella* Senftenberg 775W.,” *Appl. Microbiol.*, vol. 17, no. 1,

pp. 78–82, 1969.

[36] W. A. M. Ã. Hijnen, E. F. Beerendonk, and G. J. Medema, “Inactivation credit of UV radiation for viruses, bacteria and protozoan (oo)cysts in water: A review,” *Water Res.*, vol. 40, no. 1, pp. 3–22, 2006.

[37] C. Tseng and C. Li, “Inactivation of surface viruses by gaseous ozone,” *J. Environ. Health*, vol. 70, no. 10, pp. 56–62, Jun. 2008.

[38] J. Hudson, M. Sharma, and S. Vimalanathan, “Development of a practical method for using ozone gas as a virus decontaminating agent,” *Ozone Sci. Eng.*, vol. 31, no. 3, pp. 216–223, 2009.

[39] H. Aboubakr *et al.*, “Cold argon-oxygen plasma species oxidize and disintegrate capsid protein of feline calicivirus,” *PLoS One*, vol. 13, no. 3, p. e0194618, 2018.

[40] W. Tian and M. J. Kushner, “Atmospheric pressure dielectric barrier discharges interacting with liquid covered tissue,” *J. Phys. D. Appl. Phys.*, vol. 47, p. 165201, 2014.

[41] Y. Kimura, K. Takashima, S. Sasaki, and T. Kaneko, “Investigation on dinitrogen pentoxide roles on air plasma effluent exposure to liquid water solution,” *J. Phys. D. Appl. Phys.*, vol. 52, p. 064003, 2019.

[42] E. Wiberg, N. Wiberg, and A. Holleman, *Inorganic Chemistry.*, vol. 86, no. 2. Berlin: Academic, 2005.

[43] S. Ikawa, A. Tani, Y. Nakashima, and K. Kitano, “Physicochemical properties of bactericidal plasma-treated water,” *J. Phys. D. Appl. Phys.*, vol. 49, p. 425401, 2016.

[44] H. A. Aboubakr, U. Gangal, M. M. Youssef, S. M. Goyal, and P. J. Bruggeman, “Inactivation of virus in solution by cold atmospheric pressure plasma: Identification of chemical inactivation pathways,” *J. Phys. D. Appl. Phys.*, vol. 49, no. 20, p. 204001, 2016.

[45] M. Laroussi, “Low Temperature Plasma-Based Sterilization : Overview and State-of-the-Art,” *Plasma Process. Polym.*, vol. 2, pp. 391–400, 2005.

[46] X. Liao, D. Liu, Q. Xiang, J. Ahn, S. Chen, and X. Ye, “Inactivation mechanisms of non-thermal plasma on microbes : A review,” *Food Control*, vol. 75, pp. 83–91, 2017.

[47] S. C. Min, S. Hyeon, B. A. Niemira, J. E. Sites, G. Boyd, and A. Lacombe, “Dielectric barrier discharge atmospheric cold plasma inhibits Escherichia coli O157 : H7 , Salmonella , Listeria monocytogenes , and Tulane virus in Romaine

lettuce ☆,” *Int. J. Food Microbiol.*, vol. 237, pp. 114–120, 2016.

[48] R. N. Pereira and A. A. Vicente, “Environmental impact of novel thermal and non-thermal technologies in food processing,” *Food Res. Int.*, vol. 43, no. 7, pp. 1936–1943, 2010.

[49] D. Kingsley, D. Hoover, E. Papafragkou, and G. Richards, “Inactivation of hepatitis A virus and a calicivirus by high hydrostatic pressure,” *J. Food Prot.*, vol. 65, no. 10, pp. 1605–1609, 2002.

[50] J. Guerrero-Beltran n and G. Barbosa-Canovas, “Advantages and limitations on processing foods by UV light,” *Rev. Agaroquimica y Tecnol. Aliment.*, vol. 10, no. 3, pp. 137–147, 2004.

[51] US EPA, “The initial virucidal effectiveness test,” 2015. [Online]. Available: https://www.epa.gov/sites/production/files/2015-%0A09/documents/fcv1_initial_surf_pcol.pdf.

[52] R. Ossiboff, Y. Zhou, P. Lightfoot, B. Prasad, and J. Parker, “Conformational changes in the capsid of a calicivirus upon interaction with its functional receptor,” *J. Virol.*, vol. 84, no. 11, pp. 5550–5564, 2010.

[53] H. Aboubakr, A. El-Banna, M. Youssef, S. Al-Sohaimy, and S. Goyal, “Antiviral effects of Lactococcus lactis on feline calicivirus, a human norovirus surrogate,” *Food Environ. Virol.*, vol. 6, no. 4, pp. 282–289, 2014.

[54] K. M. Miranda, M. G. Espey, and D. A. Wink, “A Rapid , Simple Spectrophotometric Method for Simultaneous Detection of Nitrate and Nitrite,” vol. 5, no. 1, pp. 62–71, 2001.

[55] G. Eisenberg, “Colorimetric determination of hydrogen peroxide,” *Ind. Eng. Chem. Anal. Ed.*, vol. 15, no. 5, pp. 327–328, 1943.

[56] T. P. Labuza, “THE PROPERTIES OF WATER IN RELATIONSHIP TO WATER BINDING IN FOODS : A REVIEW ‘!,’” vol. 1, no. 10, pp. 167–190, 1977.

[57] R. Atkinson, D. Baulch, R. Cox, J. Crowley, and R. Hampson, “Summary of Evaluated Kinetic and Photochemical Data for Atmospheric Chemistry,” *IUPAC Subcomm. Gas Kinet. Data Eval. Atmos. Chem.*, 2001.

[58] R. Atkinson, D. Baulch, R. Cox, R. Hampson Jr., J. Kerr, and J. Troe, “Evaluated Kinetic and Photochemical Data for Atmospheric Chemistry: Supplement III,” *J. Phys. Chem. Ref. Data*, vol. 18, pp. 881–1097, 1989.

[59] M. Anbar and H. Taube, “Interaction of nitrous acid with hydrogen peroxide and

water," *J. Am. Chem. Soc.*, vol. 76, no. 24, pp. 6243–6247, 1954.

[60] B. Ahlfeld *et al.*, "Inactivation of a Foodborne Norovirus Outbreak Strain with nonthermal atmospheric pressure plasma," *MBio*, vol. 6, no. 1, pp. 1–5, 2015.

[61] G. Daeschlein *et al.*, "Plasma Medicine in Dermatology: Basic Antimicrobial Efficacy Testing as Prerequisite to Clinical Plasma Therapy," *Plasma Med.*, vol. 2, no. 1–3, pp. 33–69, 2012.

[62] S. Siddique, G. Hardy, and K. Bayliss, "Cold plasma: a potential new method to manage postharvest diseases caused by fungal plant pathogens," *Plant Pathol.*, vol. 67, no. 5, pp. 1011–1021, 2017.

[63] D. Ziuzina, S. Patil, P. J. Cullen, K. M. Keener, and P. Bourke, "Atmospheric cold plasma inactivation of Escherichia coli, Salmonella enterica serovar Typhimurium and Listeria monocytogenes inoculated on fresh produce," *Food Microbiol.*, vol. 42, pp. 109–116, 2014.

[64] B. Niemira and J. Sites, "Cold plasma inactivates Salmonella Stanley and Escherichia Coli O157:H7 inoculated on golden delicious apples," *J. Food Prot.*, vol. 71, no. 7, pp. 1357–1365, 2008.

[65] H. Lee, J. Eun, M. Chung, and S. C. Min, "Cold plasma treatment for the microbiological safety of cabbage , lettuce , and dried fi gs," *Food Microbiol.*, vol. 51, pp. 74–80, 2015.

[66] D. Bermúdez-aguirre, E. Wemlinger, P. Pedrow, G. Barbosa-cánovas, and M. Garcia-perez, "Effect of atmospheric pressure cold plasma (APCP) on the inactivation of Escherichia coli in fresh produce," *Food Control*, vol. 34, no. 1, pp. 149–157, 2013.

[67] B. Dirks, D. Dobrynin, G. Fridman, Y. Mukhin, A. Fridman, and J. J. Quinlan, "Treatment of raw poultry with nonthermal dielectric barrier discharge plasma to reduce Campylobacter jejuni and Salmonella enterica," *J. Food Prot.*, vol. 75, no. 1, pp. 22–28, 2012.

[68] A. Lacombe *et al.*, "Nonthermal inactivation of norovirus surrogates on blueberries using atmospheric cold plasma," *Food Microbiol.*, vol. 63, pp. 1–5, 2017.

[69] N. N. Misra *et al.*, "In-package atmospheric pressure cold plasma treatment of strawberries," *J. Food Eng.*, vol. 125, no. 1, pp. 131–138, 2014.

[70] J. Jean, R. Morales-Rayas, M. Anoman, and S. Lamhoujeb, "Inactivation of hepatitis A virus and norovirus surrogate in suspension and on food-contact surfaces using pulsed UV light (pulsed light inactivation of food-borne viruses),"

Food Microbiol., vol. 28, no. 3, pp. 568–572, 2011.

[71] A. Vimont, I. Fliss, and J. Jean, "Efficacy and mechanisms of murine norovirus inhibition by pulsed-light technology," *Appl. Environ. Microbiol.*, vol. 81, no. 8, pp. 2950–2957, 2015.

[72] L. Palmieri and D. Cacace, "High intensity pulsed light technology," *Emerg. Technol. Food Process. Elsevier*, pp. 279–306, 2005.

[73] S. Bover-Cid, N. Belletti, T. Aymerich, and M. Garriga, "Modelling the impact of water activity and fat content of dry-cured ham on the reduction of Salmonella enterica by high pressure processing," *Meat Sci.*, vol. 123, pp. 120–125, 2017.

[74] J. Leon *et al.*, "Randomized, double-blinded clinical trial for human norovirus inactivation in oysters by high hydrostatic pressure processing," *Appl. Environ. Microbiol.*, vol. 77, no. 15, pp. 5476–5482, 2011.

[75] J. Ahmed, H. Ramaswamy, I. Alli, and M. Ngadi, "Effect of high pressure on rheological characteristics of liquid egg," *LWT-Food Sci. Technol.*, vol. 36, no. 5, pp. 517–524, 2003.

[76] G. Park, K. Linden, and M. Sobsey, "Inactivation of murine norovirus, feline calicivirus and echovirus 12 as surrogates for human norovirus (NoV) and coliphage (F+) MS2 by ultraviolet light (254 nm) and the effect of cell association on UV inactivation," *Lett. Appl. Microbiol.*, vol. 52, no. 2, pp. 162–167, 2011.

[77] A. de Roda Husman *et al.*, "Calicivirus inactivation by nonionizing (253.7-nanometer-wavelength [UV]) and ionizing (gamma) radiation," *Appl. Environ. Microbiol.*, vol. 70, no. 9, pp. 5089–5093, 2004.

[78] S. Nuanualsuwan, T. Mariam, S. Himathongkham, and D. Cliver, "Ultraviolet inactivation of feline calicivirus, human entericviruses and coliphages," *Photochem. Photobiol.*, vol. 76, no. 4, pp. 406–410, 2002.

[79] J. Thurston-Enriquez, C. Haas, J. Jacangelo, K. Riley, and C. Gerba, "Inactivation of feline calicivirus and adenovirus type 40 by UV radiation," *Appl. Environ. Microbiol.*, vol. 69, no. 1, pp. 577–582, 2003.

[80] G. Barbosa-Canovas, M. Tapia, and M. Cano, *Novel Food Processing Technologies*, 1st ed. CRC Press, 2004.

[81] S. Bartsch, B. Lopman, S. Ozawa, A. Hall, and B. Lee, "Global economic burden of norovirus gastroenteritis," *PLoS One*, vol. 11, no. 4, p. e0151219, 2016.

[82] S. Sosnovtsev, G. Belliot, K. Chang, O. Onwudiwe, and K. Green, "Feline calicivirus VP2 is essential for the production of infectious virions," *J. Virol.*, vol.

79, no. 7, pp. 4012–4024, 2005.

[83] B. Eliasson, S. Member, and U. Kogelschatz, “Nonequilibrium Volume Plasma Chemical Processing,” vol. 19, no. 6, pp. 1063–1077, 1991.

[84] S. Okazaki *et al.*, “Raising of ozone formation efficiency in a homogeneous glow discharge plasma at atmospheric pressure,” *J. Phys. D. Appl. Phys.*, vol. 27, pp. 1985–1987, 1994.

[85] U. Kogelschatz and B. Eliasson, “Ozone generation and applications,” *Handb. Electrost. Process. Chapter 26*, no. Ed: J S Chang et al, pp. 581–605, 1995.

[86] J. M. Samaranayake, T. Namihira, S. Katsuki, and T. Sakugawa, “Pulsed streamer discharge characteristics of ozone production in dry air,” no. July 2013, 2000.